Abstracta

Ano XXVIII - N. 01

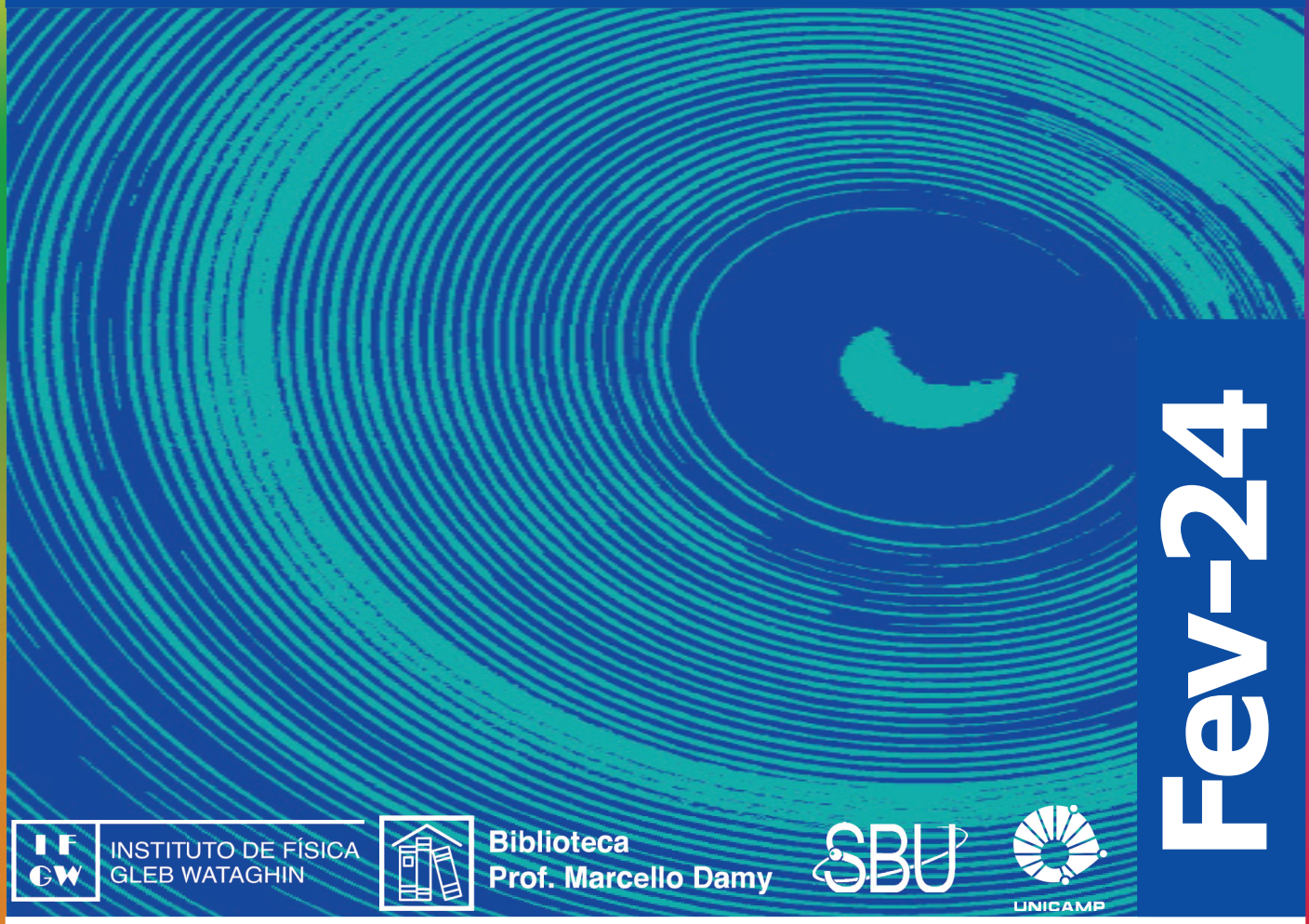

Fev-24

INSTITUTO DE FÍSICA GLEB WATAGHIN

Biblioteca Prof. Marcello Damy

SBU

UNICAMP

Artigos publicados 2023

[P322-2023] "A procedure to minimize EEG variability for BCI applications"

Melo, G. C. de; **Castellano, G.***; Forner-Cordero, A.

A Brain-Computer Interface (BCI) decodes brain activities to translate them into computer commands. Electro-encephalography is the most widely adopted technique for brain signal recording in BCIs, because of practical and safety reasons. However, EEG signals show a significant intra-subject variability, which constitutes a major challenge for BCI development. The main goal of this work is to improve a pseudo-online movement detection system using motor imagery EEG signals that simulate the BCI input. We propose a strategy that aims at minimizing the effects of the poor spatial resolution and the active reference electrode based on finding the best combinations of electrode pairs. The proposed method finds subject-specific pairs of electrodes along with signal transformations that provide the more stable results. The average accuracy across 15 subjects was 95 %. It was also seen that energy signals in the delta band (0-4 Hz) of the electrode line CCP (according to the 10-20 system) are associated to the lowest variability. The hypothesis of lower variability being associated to movement related information and therefore to higher accuracy in classification was confirmed by the results. The main conclusion is that it is possible to overcome in some level the signal variability without introducing mathematical or physical uncertainties inherent to commonly adopted approaches such as spatial filters or volume conduction modeling, for instance. The contribution of this work is the procedure to minimize EEG variability for BCI applications. The significance is the possibility to apply the procedure to any set of channels and transformations.

BIOMEDICAL SIGNAL PROCESSING AND CONTROL 89, 105745, 2023. DOI: 10.1016/j.bspc.2023.105745

[P323-2023] "A search for decays of the Higgs boson to invisible particles in events with a top-antitop quark pair or a vector boson in proton-proton collisions at √s=13TeV"

Tumasyan, A.; Adam, W.; **Chinellato, J. A.***; et al.
CMS Collaboration

Asearch for decays to invisible particles ofHiggs bosons produced in association with a top-antitop quark pair or a vector boson, which both decay to a fully hadronic final state, has been performed using proton-proton collision data collected at root s = 13 TeV by the CMS experiment at the LHC, corresponding to an integrated luminosity of 138 fb(-1). The 95% confidence level upper limit set on the branching fraction of the 125 GeV Higgs boson to invisible particles, B(H -> inv), is 0.54 (0.39 expected), assuming standard model production cross sections. The results of this analysis are combined with previous B(H -> inv) searches carried out at root s = 7, 8, and 13 TeV in complementary production modes. The combined upper limit at 95% confidence level on B(H -> inv) is 0.15 (0.08 expected).

EUROPEAN PHYSICAL JOURNAL C 83[10], 933,2023. DOI: 10.1140/epjc/s10052-023-11952-7

[P324-2023] "Adulteration of Clove Essential Oil: Detection Using an Electronic Nose with Polymeric Gas Sensors"

Graboski, A. M.; Feltes, G.; Zakrzevski, C. A.; **Shimizu, F. M.***; Steffens, J.; Paroul, N.; Steffens, C.

Food adulteration is a global concern that affects almost all the food industry. The market for clove essential oil (CEO) has also been affected by corrupt practices. As an alternative to monitoring the quality of this product, an electronic nose (e-nose) based on an array of polymeric nanocomposite gas sensors modified with different sensitive layers was applied to detect vaseline (petroleum jelly), the most common adulterant found in the CEO. Different proportions of vaseline (ranging from 3 to 100% (v/v)) were mixed with CEO samples, and the fingerprints of volatile compounds were obtained using the e-nose and Fourier transform infrared-attenuated total reflectance (FTIR-ATR) spectroscopy. Collected data were analyzed using clustering analysis (CA), principal component analysis (PCA), linear discriminant analysis (LDA), and interactive document map (IDMAP) multivariate projection techniques. These were capable of discriminating between the different percentages of adulterants. The results of this study demonstrated that chemometric tools can be successfully used as e-nose and applied to detect mislabeling and adulteration of CEO, where PCA, LDA, and IDMAP showed accuracies of 99.85, 98.30, and 99.81%, respectively. The e-nose results were consistent with the findings from density and refractive index experiments. Thus, the results obtained demonstrate that the e-nose is a promising tool for analyzing CEO adulterations, proving its potential application in the food industry due to its rapid, economical, and high-performance tool.

FOOD ANALYTICAL METHODS 17[2], 296-308, 2023. DOI: 10.1007/s12161-023-02564-8

[P325-2023] "Ag Surface Segregation in Sub-10-nm Bimetallic AuAg Nanoparticles Quantified by STEM-EDS and Machine Learning: Implications for Fine-Tuning Physicochemical Properties for Plasmonics and Catalysis Applications"

Moreira, M.*; Hillenkamp, M.*; Rodrigues, V.*; Ugarte, D.*

Mono- and multimetallic nanoparticles have been extensively studied in various fields due to their tunable physicochemical properties and potential for replacing expensive metals with more abundant and affordable ones. The chemical structure, i.e., the spatial distribution of elements inside nanoparticles, plays a crucial role in defining their properties, particularly in catalytic processes. However, accurately determining the spatial chemical distribution within sub-10-nm bimetallic nanoparticles remains a challenge. In this study, we have used scanning transmission electron microscopy associated with energy-dispersive spectroscopy to acquire hyperspectral images of gold-silver alloy nanoparticles in the 3-10-nm size range. We have quantified the chemical composition as a function of radial position; Ag enrichment toward the nanoparticle surface is robustly confirmed by statistical analysis, error bars, and nonoverlapping 3-sigma uncertainty intervals at the nanoparticle center and surface. Two complementary machine learning analyses (principal component analysis and non-negative matrix factorization) reveal that our experiments contain latent information on subtle composition variations inside the particles. The proposed data analysis procedures have also been validated by simulated data sets. These findings pave the way for more precise structural and chemical investigations of alloys on the nanoscale.

ACS APPLIED NANO MATERIALS 7[1], 1369-1378, 2023. DOI: 10.1021/acsanm.3c05495

[P326-2023] "Closing in on critical net-baryon fluctuations at LHC energies: Cumulants up to third order in Pb-Pb collisions"

Acharya, S.; Adamová, D.; **Chinellato, D. D.*; Guardiano, G. G.*; Jahnke, C.*; Takahashi, J.***; et al.
ALICE Collaboration

Fluctuation measurements are important sources of information on the mechanism of particle production at LHC energies.

This article reports the first experimental results on third--order cumulants of the net-proton distributions in Pb-Pb collisions at a center-of-mass energy root s(NN) = 5.02 TeV recorded by the ALICE detector. The results on the second--order cumulants of net-proton distributions at root s(NN) = 2.76 and 5.02TeV are also discussed in view of effects due to the global and local baryon number conservation. The results demonstrate the presence of long-range rapidity correlations between protons and antiprotons. Such correlations originate from the early phase of the collision. The experimental results are compared with HIJING and EPOS model calculations, and the dependence of the fluctuation measurements on the phase-space coverage is examined in the context of lattice quantum chromodynamics (LQCD) and hadron resonance gas (HRG) model estimations. The measured third-order cumulants are consistent with zero within experimental uncertainties of about 4% and are described well by LQCD and HRG predictions. (c) 2022 The Author. Published by Elsevier B.V. This is an open access article under the CC BY license (http://creativecommons.org/licenses/by/4.0/). Funded by SCOAP(3).

PHYSICS LETTERS B 844, 137545, 2023. DOI: 10.1016/j.physletb.2022.137545

[P327-2023] "Dense nuclear matter equation of state from heavy-ion collisions"
Sorensen, A.; Agarwal, K.; **Torrieri, G.***; et al.

The nuclear equation of state (EOS) is at the center of numerous theoretical and experimental efforts in nuclear physics. With advances in microscopic theories for nuclear interactions, the availability of experiments probing nuclear matter under conditions not reached before, endeav-ors to develop sophisticated and reliable transport simulations to interpret these experiments, and the advent of multi-messenger astronomy, the next decade will bring new opportunities for determining the nuclear matter EOS, elucidating its dependence on density, temperature, and isospin asymmetry. Among controlled terrestrial experiments, collisions of heavy nuclei at inter -mediate beam energies (from a few tens of MeV/nucleon to about 25 GeV/nucleon in the fixed-target frame) probe the widest ranges of baryon density and temperature, enabling studies of nuclear matter from a few tenths to about 5 times the nuclear saturation density and for temper-atures from a few to well above a hundred MeV, respectively. Collisions of neutron-rich isotopes further bring the opportunity to probe effects due to the isospin asymmetry. However, capitaliz-ing on the enormous scientific effort aimed at uncovering the dense nuclear matter EOS, both at RHIC and at FRIB as well as at other international facilities, depends on the continued develop-ment of state-of--the-art hadronic transport simulations. This white paper highlights the essential role that heavy-ion collision experiments and hadronic transport simulations play in understand -ing strong interactions in dense nuclear matter, with an emphasis on how these efforts can be used together with microscopic approaches and neutron star studies to uncover the nuclear EOS.

PROGRESS IN PARTICLE AND NUCLEAR PHYSICS 134, 104080, 2023. DOI: 10.1016/j.ppnp.2023.104080

[P328-2024] "Effects of quantum decoherence in a future supernova neutrino detection"

Santos, M. V. dos*; Holanda, P. C. de*; Dedin Neto, P.*; Kemp, E.*

Quantum decoherence effects in neutrinos, described by the open quantum systems formalism, serve as a gateway to explore potential new physics, including quantum gravity. Previous research extensively investigated these effects across various neutrino sources, imposing stringent constraints on the spontaneous loss of coherence. In this study, we demonstrate that even within the supernovae environment, where neutrinos are released as incoherent states, quantum decoherence could influence the flavor equipartition of 3v mixing. Additionally, we examine the potential energy dependence of quantum decoherence parameters (F = F0(E=E0)n) with different power laws (n = 0; 2; 5=2). Our findings indicate that future-generation detectors (DUNE, Hyper-K, and JUNO) can significantly constrain quantum decoherence effects under different scenarios. For a supernova located 10 kpc away from Earth, if no quantum decoherence is observed, DUNE could potentially establish 3u bounds of F <= 6.2 x 10-14 eV in the normal mass hierarchy (NH) scenario, while Hyper-K would impose a 2u limit of F <= 3.6 x 10-14 eV for the inverted mass hierarchy (IH) with n = 0-assuming no energy exchange between the neutrino subsystem and nonstandard environment. These limits become even more restrictive for a closer supernova. When we relax the assumption of energy exchange, for a 10 kpc distance, DUNE could establish a 3u limit of F8 <= 4.2 x 10-28 eV for NH, while Hyper-K could constrain F8 <= 1.3 x 10-27 eV for IH (n = 0) with 2u, which would be orders of magnitude stronger than the bounds reported to date. Furthermore, we examine the impact of neutrino loss during propagation for future supernova detection.

PHYSICAL REVIEW D 108[10], 103032, 2023. DOI: 10.1103/PhysRevD.108.103032

[P329-2023] "Electron impact electronic excitation of benzene: Theory and experiment"

Falkowski, A.G.*; Costa, R.F. da; **Lima, M.A.P.***; Cadena, A. de A.; Pocoroba, R.; Jones, R.; Mathur, M.; Childers, J.G.; Khakoo, M.A.; Kossoski, F.

We report experimental differential cross sections (DCSs) for electron impact excitation of bands I to V of benzene at incident energies of 10, 12.5, 15, and 20 eV. They are compared to calculations using the Schwinger multichannel method while accounting for up to 437 open channels. For intermediate scattering angles, the calculations reveal that the most intense band (V) emerges from surprisingly similar contributions from all its underlying states (despite some preference for the dipole-allowed transitions). They further shed light on intricate multichannel couplings between the states of bands I to V and higher-lying Rydberg states. In turn, the measurements support a vibronic coupling mechanism for excitation of bands II and IV and also show an unexpected forward peak in the spin-forbidden transition accounting for band III. Overall, there is decent agreement between theory and experiment at intermediate angles and at lower energies and in terms of the relative DCSs of the five bands. Discrepancies between the present and previous experiment regarding bands IV and V draw attention to the need of additional experimental investigations. We also report measured DCSs for vibrational excitation of combined C-H stretching modes.

JOURNAL OF CHEMICAL PHYSICS 159[19], 194301, 2023. DOI: 10.1063/5.0173024

[P330-2023] "Energy dependence of coherent photonuclear production of J/ψ mesons in ultra-peripheral Pb-Pb collisions at √sNN=5.02 TeV"

Acharya, S.; Adamova, D.; **Chinellato, D. D.*; Guardiano, G. G.*; Jahnke, C.*; Liveraro, G. S. S.*; Takahashi, J.***; et al.
ALICE Collaboration

The cross section for coherent photonuclear production of J/psi is presented as a function of the electromagnetic dissociation (EMD) of Pb. The measurement is performed with the ALICE detector in ultra-peripheral Pb-Pb collisions at a centre-of-mass energy per nucleon pair of root s(NN) = 5.02 TeV.

Cross sections are presented in five different J/psi rapidity ranges within |y| < 4, with the J/psi reconstructed via its dilepton decay channels. In some events the J/psi is not accompanied by EMD, while other events do produce neutrons from EMD at beam rapidities either in one or the other beam direction, or in both. The cross sections in a given rapidity range and for different configurations of neutrons from EMD allow for the extraction of the energy dependence of this process in the range 17 < W-gamma Pb,W-n < 920 GeV, where W--gamma Pb,W-n is the centre-of-mass energy per nucleon of the gamma Pb system. This range corresponds to a Bjorken-x interval spanning about three orders of magnitude: 1.1 x 10(-5) < x < 3.3 x 10(-2). In addition to the ultra-peripheral and photonuclear cross sections, the nuclear suppression factor is obtained. These measurements point to a strong depletion of the gluon distribution in Pb nuclei over a broad, previously unexplored, energy range. These results, together with previous ALICE measurements, provide unprecedented information to probe quantum chromodynamics at high energies.

JOURNAL OF HIGH ENERGY PHYSICS [10], 119, 2023. DOI: 10.1007/JHEP10(2023)119

[P331-2023] "Enhanced spin current transmissivity in Pt/CoFe2O4 bilayers with thermally induced interfacial magnetic modification"

Gamino, M.; Oliveira, A. B.; Maior, D. S.; **Ribeiro, P. R. T.***; Machado, F. L. A.; Mori, T. J. A.; Correa, M. A.; Bohn, F.; Rodriguez-Suarez, R. L.; Fontcuberta, J.; Rezende, S. M.

We report on processes of generation of spin current and conversion into charge current in CoFe2O4/Pt bilayers by means of spin Hall magnetoresistance (SMR) and spin Seebeck effect (SSE) experiments. Specifically, we explore (001) full-textured CoFe2O4 (CFO) thin films grown onto (001)-oriented SrTiO3 substrates, covered with Pt layers deposited under two different conditions: one at room temperature and another at high temperature (400 degrees C). The x-ray absorption spectroscopy measurements indicate that the Pt layer deposited at high temperature induces an interfacial magneticlike phase (Fe,Co)-Pt alloy, which influences the magnetic behavior of the structure and is responsible for the enhancement of the spin transmission at the interface. By analyzing the SMR data, we conclude that collinear and noncollinear magnetic domains coexist at the CFO-(Fe,Co)-Pt interface. By combining the data from the SMR and SSE measurements, we obtain the ratios between the values of the spin Hall angle (theta SH) and between the ones of the spin-mixing conductance (g up arrow down arrow that while the value of theta SH decreases by one--half with the heat treatment, the value of g up arrow down arrow one order of magnitude. We interpret the increase of g up arrow down arrow eff in terms of unexpected magnetic reconstructions, which produce an enhancement of the magnetic moment arisen at the interface. Since the spin-mixing conductance determines the efficiency of the spin current transmission through the interface, the spinel ferrite cobalt in contact with a normal metal with a suitable heat treatment becomes a promising material for spintronics device applications.

PHYSICAL REVIEW B 108[22], 224402, 2023. DOI: 10.1103/PhysRevB.108.224402

[P332-2023] "Evidence for four-top quark production in proton-proton collisions at √s=13 TeV"

Tumasyan, A.; Adam, W.; **Chinellato, J. A.***; et al.
CMS Collaboration

The production of four top quarks (tt over bar tt over bar) is studied with LHC proton-proton collision data samples collected by the CMS experiment at a center-of-mass energy of 13 TeV, and corresponding to integrated luminosities of up to 138 fb-1. Events that have no leptons (all-hadronic), one lepton, or two oppositesign leptons (where lepton refers only to prompt electrons or prompt muons) are considered. This is the first tt over bar tt over bar measurement that includes the all-hadronic final state. The observed significance of the tt over bar tt over bar signal in these final states of 3.9 standard deviations (1.5 expected) provides evidence for tt over bar tt over bar production, with a measured cross section of 36+12 signal significance is 4.0 standard deviations (3.2 expected). The combination returns an observed cross section of 17 +/- 4 (stat) +/- 3 (syst) fb, which is consistent with the standard model prediction.

PHYSICS LETTERS B 844, 138076, 2023. DOI: 10.1016/j.physletb.2023.138076

[P333-2023] "Exploration of an impedimetric electronic tongue and chemometrics for characterization of black tea from different origins"

Raj, D.R.K.; Ferreira, M.V. da S.; **Braunger, M.L.*; Riul Jr., A.***; Thomas, J.; Barbin, D.F.

Tea is the second most consumed beverage globally due to its flavour and therapeutical properties. The geographical location is a key indicator for distinct tea quality as it influences tea chemical composition, and there are various grades in the market, demanding a rapid assessment of tea quality grade for economic purposes. We have developed and applied a multi-sensing impedimetric device (electronic tongue) based on Layer-byLayer (LbL) nanostructured materials as sensing units in the discrimination of black tea based on chemical composition. PLS-DA and PLSR were applied to the data obtained from the electronic tongue to classify samples according to chemical composition related to country of origin and to predict total flavonoids, total polyphenols and caffeine content. Total flavonoids and caffeine content could be predicted using partial least squares regression (PLSR) with coefficients of determination (R2P) of 0.77 and 0.71, respectively. The results show the potential of this impedimetric e-tongue for discriminating teas based on chemical composition.

JOURNAL OF FOOD COMPOSITION AND ANALYSIS 123, 105535, 2023. DOI: 10.1016/j.jfca.2023.105535

[P334-2023] "Fibrillary Arrangement of Elongated, Almost Parallel Aggregates of Hydrophobic and Hydrophilic Domains Forming the Nafion Surface Structure Improved Contrast Atomic Force Microscopy Images"

Teschke, O.*; Burguim, J. A. F.*; Gomes, W. E.; **Soares, D. M.***

A significant improvement in spatial resolution is reported in Nafion surface maps when compared to previous atomic force microscopy images of the Nafion surface scanned in air. The technique ability is to generate maps showing approximately few nanometer (similar to 2-5 nm) patterns to the long fiber length (>2 mu m). Atomic force microscopy force vs separation curve profiles registered in water are used to characterize the surface hydrophobic and hydrophilic domains. Initially, Nafion surfaces were imaged in air for comparison and then immersed in water. Nafion surfaces immersed in water display a matrix of hydrophilic and hydrophobic regions with fibrillary structure dimensions of similar to 40 nm formed by fiber pairs.

Ribbons formed by two pairs with diameters of similar to 83 nm are separated by larger channels.

ACS OMEGA 8[51], 49073-49079, 2023. DOI: 10.1021/acsomega.3c06927

[P335-2023] "First measurement of the forward rapidity gap distribution in pPb collisions at √sNN=8.16 TeV sNN"

Tumasyan, A.; Adam, W.; **Chinellato, J. A.***; **Tonelli Manganote, E. J.***; et al.
CMS Collaboration

For the first time at LHC energies, the forward rapidity gap spectra from proton-lead collisions for both proton and lead dissociation processes are presented. The analysis is performed over 10.4 units of pseudorapidity at a center-of-mass energy per nucleon pair of ffisffi than in previous measurements of diffractive production in proton-nucleus collisions. For lead dissociation processes, which correspond to the pomeron-lead event topology, the EPOS-LHC generator predictions are a factor of 2 below the data, but the model gives a reasonable description of the rapidity gap spectrum shape. For the pomeron-proton topology, the EPOS-LHC, QGSJET II, and HIJING predictions are all at least a factor of 5 lower than the data. The latter effect might be explained by a significant contribution of ultraperipheral photoproduction events mimicking the signature of diffractive processes. These data may be of significant help in understanding the high energy limit of quantum chromodynamics and for modeling cosmic ray air showers.

PHYSICAL REVIEW D 108[9], 092004, 2024. DOI: 10.1103/PhysRevD.108.092004

[P336-2023] "First measurement of Ω0c production in pp collisions at √s=13 TeV"

Acharya, S.; Adamová, D.; **Chinellato, D. D.*; Guardiano, G. G.*; Jahnke, C.*; Takahashi, J.***; et al.
ALICE Collaboration

The inclusive production of the charm-strange baryon Omega(0)(c) is measured for the first time via its hadronic decay into Omega(-)pi(+) at midrapidity (|y| < 0.5) in proton-proton (pp) collisions at the centre-of-mass energy root s = 13 TeV with the ALICE detector at the LHC. The transverse momentum (p(T)) differential cross section multiplied by the branching ratio is presented in the interval 2 < p(T) < 12 GeV/c. The p(T) dependence of the Omega(0)(c)-baryon production relative to the prompt D-0-meson and to the prompt (sic)(0)(c)-baryon production is compared to various models that take different hadronisation mechanisms into consideration. In the measured p(T) interval, the ratio of the p(T)-integrated cross sections of Omega(0)(c) and prompt Lambda(+)(c)baryons multiplied by the Omega(-)pi(+) branching ratio is found to be larger by a factor of about 20 with a significance of about 4 sigma when compared to e(+)e(-) collisions. (c) 2022 The Author(s). Published by Elsevier B.V. This is an open access article under the CC BY license (http://creativecommons .org /licenses /by /4 .0/). Funded by SCOAP3.

PHYSICS LETTERS B 846, 137625, 2023. DOI: 10.1016/j.physletb.2022.137625

[P337-2023] "Generalized Bell Scenarios: Disturbing Consequences on Local-Hidden-Variable Models"

Mazzari, A.*; Ruffolo, G.*; Vieira, C.; **Temistocles, T.*; Rabelo, R.***; Cunha, M.T.

Bell nonlocality and Kochen-Specker contextuality are among the main topics in the foundations of quantum theory. Both of them are related to stronger-than-classical correlations, with the former usually referring to spatially separated systems, while the latter considers a single system. In recent works, a unified framework for these phenomena was presented. This article reviews, expands, and obtains new results regarding this framework. Contextual and disturbing features inside the local models are explored, which allows for the definition of different local sets with a non-trivial relation among them. The relations between the set of quantum correlations and these local sets are also considered, and post--quantum local behaviours are found. Moreover, examples of correlations that are both local and non-contextual but such that these two classical features cannot be expressed by the same hidden variable model are shown. Extensions of the Fine-Abramsky-Brandenburger theorem are also discussed.

ENTROPY 25[9], 1276, 2023. DOI: 10.3390/e25091276

[P338-2023] "Global Room-Temperature Superconductivity in Graphite"

Kopelevich, Y.*; Torres, J.*; Silva, R. da*; Oliveira, F.*; Diamantini, M. C.; Trugenberger, C.; Vinokur, V.

Room temperature superconductivity under normal conditions has been a major challenge of physics and material science since its discovery. Here the global room-temperature superconductivity observed in cleaved highly oriented pyrolytic graphite carrying dense arrays of nearly parallel surface line defects is reported. The multiterminal measurements performed at the ambient pressure in the temperature interval 4.5 K <= T <= 300 K and at magnetic fields 0 <= B <= 9 T applied perpendicular to the basal graphitic planes reveal that the superconducting critical current I-c(T, B) is governed by the normal state resistance R-N(T, B) so that I-c(T, B) is proportional to 1/R-N(T, B). Magnetization M(T, B) measurements of superconducting screening and hysteresis loops together with the critical current oscillations with temperature that are characteristic for superconductor-ferromagnet-superconductor Josephson chains, provide strong support for the occurrence of superconductivity at T > 300 K. A theory of global superconductivity emerging in the array of linear structural defects is developed which well describes the experimental findings and demonstrate that global superconductivity arises as a global phase coherence of superconducting granules in linear defects promoted by the stabilizing effect of underlying Bernal graphite via tunneling coupling to the three dimensional (3D) material.

ADVANCED QUANTUM TECHNOLOGIES, 2023. DOI: 10.1002/qute.202300230 **Early Access Date: DEC 2023**

[P339-2023] "Harnessing Small-Molecule Analyte Detection in Complex Media: Combining Molecularly Imprinted Polymers, Electrolytic Transistors, and Machine Learning"

Lelis, G. C.; Fonseca, W. T.; Lima, A. H. de; Okazaki, A. K.; Figueiredo, E. C.; **Riul Jr., A.***; Schleder, G. R.; Samorì, P.; **Oliveira, R. F. de***

Small-molecule analyte detection is key for improving quality of life, particularly in health monitoring through the early detection of diseases. However, detecting specific markers in complex multicomponent media using devices compatible with point-of-care (PoC) technologies is still a major challenge. Here, we introduce a novel approach that combines molecularly imprinted polymers (MIPs), electrolyte--gated transistors (EGTs) based on 2D materials, and machine learning (ML) to detect hippuric acid (HA) in artificial urine, being a critical marker for toluene intoxication, parasitic infections, and kidney and bowel inflammation.

Reduced graphene oxide (rGO) was used as the sensory material and molecularly imprinted polymer (MIP) as supramolecular receptors. Employing supervised ML techniques based on symbolic regression and compressive sensing enabled us to comprehensively analyze the EGT transfer curves, eliminating the need for arbitrary signal selection and allowing a multivariate analysis during HA detection. The resulting device displayed simultaneously low operating voltages (<0.5 V), rapid response times (<= 10 s), operation across a wide range of HA concentrations (from 0.05 to 200 nmol L-1), and a low limit of detection (LoD) of 39 pmol L-1. Thanks to the ML multivariate analysis, we achieved a 2.5-fold increase in the device sensitivity (1.007 mu A/nmol L-1) with respect to the human data analysis (0.388 mu A/nmol L-1). Our method represents a major advance in PoC technologies, by enabling the accurate determination of small-molecule markers in complex media via the combination of ML analysis, supramolecular analyte recognition, and electrolytic transistors.

ACS APPLIED MATERIALS & INTERFACES, 2023. DOI: 10.1021/acsami.3c16699 **Early Access Date: DEC 2023**

[P340-2023] "Higher-order correlations between different moments of two flow amplitudes in Pb-Pb collisions at √sNN=5.02 TeV"

Acharya, S.; Adamová, D.; **Chinellato, D. D.*; Guardiano, G. G.*; Jahnke, C.*; Liveraro, G. S. S.*; Takahashi, J.***; et al.
ALICE Collaboration

The correlations between different moments of two flow amplitudes, extracted with the recently developed asymmetric cumulants, are measured in Pb-Pb collisions at root sNN = 5.02 TeV recorded by the ALICE detector at the CERN Large Hadron Collider. The magnitudes of the measured observables show a dependence on the different moments as well as on the collision centrality, indicating the presence of nonlinear response in all even moments up to the eighth. Furthermore, the higher-order asymmetric cumulants show different signatures than the symmetric and lower-order asymmetric cumulants. Comparisons with state-of-the-art event generators using two different parametrizations obtained from Bayesian optimization show differences between data and simulations in many of the studied observables, indicating a need for further tuning of the models behind those event generators. These results provide new and independent constraints on the initial conditions and transport properties of the system created in heavy-ion collisions.

PHYSICAL REVIEW C 108[5], 055203, 2023. DOI: 10.1103/PhysRevC.108.055203

[P341-2023] "Hydrogen atom/molecule adsorption on 2D metallic porphyrin: A first-principles study"

Tromer, R. M.*; Felix, I. M.; **Felix, L.C.*;** Machado, L. D.; Woellner, C. F.; **Galvao, D. S.***

Hydrogen is a promising element for applications in new energy sources like fuel cells. One key issue for such applications is storing hydrogen. And, to improve storage capacity, understanding the interaction mechanism between hydrogen and possible storage materials is critical. This work uses DFT simulations to comprehensively investigate the adsorption mechanism of H/H2 on the 2D metallic porphyrins with one transition metal in its center. Our results suggest that the mechanism for adsorption of H (H2) is chemisorption (physisorption). The maximum adsorption energy for atomic hydrogen was -3.7 eV for 2D porphyrins embedded with vanadium or chromium atoms. Our results also revealed charge transfer of up -0.43 e to chemisorbed H atoms. In contrast, the maximum adsorption energy calculated for molecular hydrogen was -122.5 meV for 2D porphyrins embedded with scandium atoms. Furthermore, charge transfer was minimal for physisorption. Finally, we also determined that uniaxial strain has a minimal effect on the adsorption properties of 2D metallic porphyrins.

CHEMICAL PHYSICS 577, 112142, 2023. DOI: 10.1016/j.chemphys.2023.112142

[P342-2023] "Impact of cross-section uncertainties on supernova neutrino spectral parameter fitting in the Deep Underground Neutrino Experiment"

Abud, A. A.; Abi, B.; A**driano, C.*; Bazetto, M. C. Q.*; Aguiar, R. de*; Almeida, P. de*; Holanda, P. C. de*; Souza, G. de*; Gelli, B.*; Giammaria, P.*; Guzzo, M. M.*; Kemp, E.*; Machado, A. A.*; Peres, O. L. G.*; Pimentel, V. L.*; Prakash, S.*; Segreto, E.*;** et al.
DUNE Collaboration

A primary goal of the upcoming Deep Underground Neutrino Experiment (DUNE) is to measure the O(10) MeV neutrinos produced by a Galactic core-collapse supernova if one should occur during the lifetime of the experiment. The liquid-argon-based detectors planned for DUNE are expected to be uniquely sensitive to the ve component of the supernova flux, enabling a wide variety of physics and astrophysics measurements. A key requirement for a correct interpretation of these measurements is a good understanding of the energy-dependent total cross section a(Ev) for charged-current ve absorption on argon. In the context of a simulated extraction of supernova ve spectral parameters from a toy analysis, we investigate the impact of a(Ev) modeling uncertainties on DUNE's supernova neutrino physics sensitivity for the first time. We find that the currently large theoretical uncertainties on a(Ev) must be substantially reduced before the ve flux parameters can be extracted reliably; in the absence of external constraints, a measurement of the integrated neutrino luminosity with less than 10% bias with DUNE requires a(Ev) to be known to about 5%. The neutrino spectral shape parameters can be known to better than 10% for a 20% uncertainty on the cross-section scale, although they will be sensitive to uncertainties on the shape of a(Ev). A direct measurement of low-energy ve-argon scattering would be invaluable for improving the theoretical precision to the needed level.

PHYSICAL REVIEW D 107[11], 112012, 2023. DOI: 10.1103/PhysRevD.107.112012

[P343-2023] "Incoherent electronic band states in Mn-substituted BaFe2As2"

Cantarino, M. R. **Pakuszewski, K. R.***; Salzmann, B.; Moya, P. H. A.; Silva Neto, W. R. da; **Freitas, G. S.*; Pagliuso, P. G.***; Brito, W. H.; Monney, C.; **Adriano, C.***; Garcia, F. A.

Chemical substitution is commonly used to explore new ground states in materials, yet the role of disorder is often overlooked. In Mn-substituted BaFe2As2 (MnBFA), superconductivity (SC) is absent, despite being observed for nominal hole-doped phases. Instead, a glassy magnetic phase emerges, associated with the S = 5/2 Mn local spins. In this work, we present a comprehensive investigation of the electronic structure of MnBFA using angle-resolved photoemission spectroscopy (ARPES). We find that Mn causes a small and orbital-specific reduction of the electron pockets, only partially disrupting nesting conditions. Based upon the analysis of the spectral properties, we observe, for all bands, an increase in the electronic scattering rate as a function of Mn content. This is interpreted as increasing band incoherence, which we propose as the primary contributor to the suppression of the magnetic order in MnBFA. This finding connects the MnBFA electronic band structure properties to the glassy magnetic behavior observed in these materials and suggests that SC is absent because of the collective magnetic impurity behavior that scatters the Fe-derived excitations.

Additionally, our analysis shows that the binding energy (EB) dependence of the imaginary part of the self-energy [ImE(EB)] is best described by a fractional scaling (ImE(EB) proportional to root-EB). These results indicate that Mn tunes MnBFA into an electronic disordered phase between the correlated Hund's metal in BaFe2As2 and the Hund's insulator in BaMn2As2.

PHYSICAL REVIEW B 108[24], 245124, 2023. DOI: 10.1103/PhysRevB.108.245124

[P344-2023] "K*(892)0 and φ(1020) production in p-Pb collisions at √sNN<=8.16 TeV

Acharya, S. **Chinellato, D. D.*; Guardiano, G. G.*; Jahnke, C.*; Takahashi, J,***; et al.
ALICE Collaboration

The production of K*(892)(0) and phi(1020) resonances has been measured in p-Pb collisions at root s(NN) = 8.16 TeV using the ALICE detector. Resonances are reconstructed via their hadronic decay channels in the rapidity interval -0.5 < y < 0 and the transverse momentum spectra are measured for various multiplicity classes up to p(T) = 20 GeV/c for K*(892)0 and p(T) = 16 GeV/c for 0(1020). The p(T)-integrated yields and mean transverse momenta are reported and compared with previous results in pp, p-Pb and Pb-Pb collisions. The x(T) scaling for K*(892)(0) and phi(1020) resonance production is newly tested in p-Pb collisions and found to hold in the high-pT region at Large Hadron Collider energies. The nuclear modification factors (RpPb) as a function of pT for K*(0) and phi at root s(NN) = 8.16 TeV are presented along with the new R-pPb measurements of K*(0), phi, Xi, and Omega at root s(NN) = 5.02 TeV. At intermediate pT (2-8 GeV/c), R-pPb of Xi, Omega show a Cronin-like enhancement, while K*(0) and phi show no or little nuclear modification. At high p(T) (>8 GeV/c), the R-pPb values of all hadrons are consistent with unity within uncertainties. The R-pPb of K*(892)(0) and phi(1020) at root s(NN) = 8.16 and 5.02 TeV show no significant energy dependence.

PHYSICAL REVIEW C 107[5], 055201, 2023. DOI: 10.1103/PhysRevC.107.055201

[P345-2023] "Measurement of beauty-strange meson production in Pb-Pb collisions at √sNN=5.02 TeV via non-prompt Ds+ mesons"

Acharya, S.; Adamová, D.; **Chinellato, D. D.*; Guardiano, G. G.*; Jahnke, C.*; Takahashi, J,***; et al.
ALICE Collaboration

The production yields of non-prompt D-s(+) smesons, namely D-s(+) smesons from beauty-hadron decays, were measured for the first time as a function of the transverse momentum (p(T)) at midrapidity (|y| < 0.5) in central and semi-central Pb-Pb collisions at a centre-of-mass energy per nucleon pair root s(NN)= 5.02TeVwith the ALICE experiment at the LHC. The D-s(+) smesons and their charge conjugates were reconstructed from the hadronic decay channel D-s(+) -> phi pi+, with phi -> K- K+, in the 4 < pT< 36GeV/cand 2 < pT< 24GeV/cintervals for the 0-10% and 30-50% centrality classes, respectively. The measured yields of non-prompt D-s(+) smesons are compared to those of prompt D-s(+) sand non-prompt D-0 mesons by calculating the ratios of the production yields in Pb-Pb collisions and the nuclear modification factor R-AA. The ratio between the R-AA of non-prompt D-s(+) sand prompt D-s(+) smesons, and that between the R-AA of non--prompt D-s(+) sand non-prompt D-0 mesons in central Pb--Pb collisions are found to be on average higher than unity in the 4 < p(T) < 12GeV/c interval with a statistical significance of about 1.6 sigma and 1.7 sigma, respectively. The measured R-AA ratios are compared with the predictions of theoretical models of heavy-quark transport in a hydrodynamically expanding QGP that incorporate hadronisation via quark recombination.

PHYSICS LETTERS B 846, 137561, 2023. DOI: 10.1016/j.physletb.2022.137561

[P346-2023] "Measurement of differential cross sections for the production of a Z boson in association with jets in proton-proton collisions at √s=13 TeV"

Tumasyan, A.; Adam, W.; **Chinellato, J. A.***; et al.
CMS Collaboration

A measurement is presented of the production of Z bosons that decay into two electrons or muons in association with jets, in proton-proton collisions at a center-of-mass energy of 13 TeV. The data were cross sections are measured as a function of the transverse momentum (pT) of the Z boson and the transverse momentum and rapidities of the five jets with largest pT. The jet multiplicity distribution is measured for up to eight jets. The hadronic activity in the events is estimated using the scalar sum of the pT of all the jets. All measurements are unfolded to the stable-particle level and compared with predictions from various Monte Carlo event generators, as well as with expectations at leading and next--to-leading orders in perturbative quantum chromodynamics.

PHYSICAL REVIEW D 108[5], 052004,2023. DOI: 10.1103/PhysRevD.108.052004

[P347-2023] "Measurement of inclusive J/ψ pair production cross section in pp collisions at √s=13 TeV"

Acharya, S.; Adamova, D.; **Chinellato, D. D.*; Guardiano, G. G.*; Jahnke, C.*; Takahashi, J.***; et al.
ALICE Collaboration

The production cross section of inclusive J/psi. pairs in pp collisions at a center-of-mass energy root s = 13 TeV is measured with ALICE. The measurement is performed for J/psi. in the rapidity interval 2.5 < y < 4.0 and for transverse momentum pT > 0. The production cross section of inclusive J/G. pairs is reported to be 10.3 +/- 2.3 (stat.) +/- 1.3 (syst.) nb in this kinematic interval. The contribution from nonprompt J/psi. (i.e., originated from beauty-hadron decays) to the inclusive sample is evaluated. The effective double-parton scattering cross section is computed, neglecting the single-parton scattering contribution.

PHYSICAL REVIEW C 108[4], 045203, 2023. DOI: 10.1103/PhysRevC.108.045203

[P348-2023] "Measurement of non-prompt D0-meson elliptic flow in Pb-Pb collisions at √sNN=5.02 TeV"

Acharya, S.; Adamová, D.; **Chinellato, D. D.*; Guardiano, G. G.*; Jahnke, C.*; .; Liveraro, G. S. S.*; Takahashi, J,***; et al.
ALICE Collaboration

The elliptic flow (v(2)) of D-0 mesons from beauty-hadron decays (non-prompt D-0) was measured in midcentral (30-50%) Pb-Pb collisions at a centre-of-mass energy per nucleon pair root sNN=5.02 TeV with the ALICE detector at the LHC. The D0 mesons were reconstructed at midrapidity (|y|<0.8) from their hadronic decay D-0 -> K-pi(+), in the transverse momentum interval 2<p(T)<12 GeV/c. The result indicates a positive v2 for non-prompt D0 mesons with a significance of 2.7 sigma.

The non-prompt D0-meson v(2) is lower than that of prompt non-strange D mesons with 3.2 sigma significance in 2<p(T)<8GeV/c, and compatible with the v(2) of beauty-decay electrons. Theoretical calculations of beauty-quark transport in a hydrodynamically expanding medium describe the measurement within uncertainties.

EUROPEAN PHYSICAL JOURNAL C 83[12], 1123, 2023. DOI: 10.1140/epjc/s10052-023-12259-3

[P349-2023] "Measurement of the Dependence of the Hadron Production Fraction Ratios fs/fu and fd/fu on B Meson Kinematic Variables in Proton-Proton Collisions at √s=13 TeV"

Tumasyan, A.; Adam, W.; **Chinellato, J. A.***; et al.

The dependence of the ratio between the B-s(0) and B+ hadron production fractions, f(s)/f(u), on the transverse momentum (p(T)) and rapidity of the B mesons is studied using the decay channels B-s(0) -> J/psi phi and B+ -> J/psi K+. The analysis uses a data sample of proton-proton collisions at a center-of--mass energy of 13 TeV, collected by the CMS experiment in 2018 and corresponding to an integrated luminosity of 61.6 fb(-1). The f(s)/f(u) ratio is observed to depend on the B p(T) and to be consistent with becoming asymptotically constant at large p(T). No rapidity dependence is observed. The ratio of the B-0 to B+ meson production fractions, f(d)/f(u), is also measured, for the first time in proton-proton collisions, using the B-0 -> J/psi K*(0) decay channel. The result is found to be within 1 standard deviation of unity and independent of p(T) and rapidity, as expected from isospin invariance.

PHYSICAL REVIEW LETTERS 131[12], 121901, 2023. DOI: 10.1103/PhysRevLett.131.121901

[P350-2023] "Measurement of the mass dependence of the transverse momentum of lepton pairs in Drell-Yan production in proton-proton collisions at √s=13 TeV"

Tumasyan, A.; Adam, W.; **Chinellato, J. A.***; et al.
CMS Collaboration

The double differential cross sections of the Drell-Yan lepton pair (l(+)l(-), dielectron or dimuon) production are measured as functions of the invariant mass m(ll), transverse momentum p(T)(ll), and phi(eta)*. The phi(eta)* observable, derived from angular measurements of the leptons and highly correlated with p(T)(ll), is used to probe the low-p(T)(ll) region in a complementary way. Dilepton masses up to 1 TeV are investigated. Additionally, a measurement is performed requiring at least one jet in the final state. To benefit from partial cancellation of the systematic uncertainty, the ratios of the differential cross sections for various m(ll) ranges to those in the Z mass peak interval are presented. The collected data correspond to an integrated luminosity of 36.3 fb(-1) of proton-proton collisions recorded with the CMS detector at the LHC at a centre-of-mass energy of 13 TeV. Measurements are compared with predictions based on perturbative quantum chromodynamics, including soft-gluon resummation.

EUROPEAN PHYSICAL JOURNAL C 83[7], 628, 2023. DOI: 10.1140/epjc/s10052-023-11631-7

[P351-2023] "Measurement of the non-prompt D-meson fraction as a function of multiplicity in proton-proton collisions at √s=13 TeV"

Acharya, S.; Adamova, D.; **Chinellato, D. D.*; Guardiano, G. G.*; Jahnke, C.*; Takahashi, J.***; et al.
ALICE Collaboration

The fractions of non-prompt (i.e. originating from beauty-hadron decays) D-0 and D+ mesons with respect to the inclusive yield are measured as a function of the charged-particle multiplicity in proton-proton collisions at a centre-of-mass energy of root s = 13 TeV with the ALICE detector at the LHC. The results are reported in intervals of transverse momentum (pT) and integrated in the range 1 < p(T) < 24 GeV/c. The fraction of non-prompt D-0 and D+ mesons is found to increase slightly as a function of p(T) in all the measured multiplicity intervals, while no significant dependence on the charged-particle multiplicity is observed. In order to investigate the production and hadronisation mechanisms of charm and beauty quarks, the results are compared to PYTHIA 8 as well as EPOS 3 and EPOS 4 Monte Carlo simulations, and to calculations based on the colour glass condensate including three-pomeron fusion.

JOURNAL OF HIGH ENERGY PHYSICS [10], 092, 2023. DOI: 10.1007/JHEP10(2023)092

[P352-2023] "Measurement of the top quark mass using a profile likelihood approach with the lepton plus jets final states in proton-proton collisions at √s=13TeV"

Tumasyan, A.; Adam, W.; **Chinellato, J. A.***; et al.
CMS Collaboration

The mass of the top quark is measured in 36.3 fb(-1) of LHC proton-proton collision data collected with the CMS detector at root s = 13 TeV. The measurement uses a sample of top quark pair candidate events containing one isolated electron or muon and at least four jets in the final state. For each event, the mass is reconstructed from a kinematic fit of the decay products to a top quark pair hypothesis. A profile likelihood method is applied using up to four observables per event to extract the top quark mass. The top quark mass is measured to be 171.77 +/- 0.37 GeV. This approach significantly improves the precision over previous measurements.

EUROPEAN PHYSICAL JOURNAL C 83[10], 963, 2023. DOI: 10.1140/epjc/s10052-023-12050-4

[P353-2023] "Measurement of the Λ hyperon lifetime"

Acharya, S.; Adamova, D.; **Chinellato, D. D.*; Guardiano, G. G.*; Jahnke, C.*; Takahashi, J.***; et al.
ALICE Collaboration

A new, more precise measurement of the. hyperon lifetime is performed using a large data sample of Pb-Pb collisions at root s(NN) = 5.02 TeV with ALICE. The Lambda and (Lambda) over bar hyperons are reconstructed at midrapidity using their two--body weak decay channel Lambda -> p + pi(-) and (Lambda) over bar -> (p) over bar + pi(+). The measured value of the. lifetime is tau(Lambda) = [261.07 +/- 0.37(stat.) +/- 0.72o(syst)] ps. The relative difference between the lifetime of Lambda and (Lambda) over bar, which represents an important test of CPT invariance in the strangeness sector, is also measured. The obtained value (tau(Lambda) - tau((Lambda) over bar))/ tau(Lambda) = (0.0013 +/- 0.0028(stat.) +/- 0.0021(syst.) is consistent with zero within the uncertainties. Both measurements of the. hyperon lifetime and of the relative difference between tau(Lambda) and tau((Lambda) over bar) are in agreement with the corresponding world averages of the Particle Data Group and about a factor of three more precise.

PHYSICAL REVIEW D 108[3], 032009, 2023. DOI: 10.1103/PhysRevD.108.032009

[P354-2023] "Measurements of azimuthal anisotropies at forward and backward rapidity with muons in high-multiplicity p-Pb collisions at √sNN=8.16 TeV"

Acharya, S.; Adamová, D.; **Chinellato, D. D.*; Guardiano, G. G.*; Jahnke, C.*; Takahashi, J.*;** et al.

The study of the azimuthal anisotropy of inclusive muons produced in p-Pb collisions at root sNN = 8.16 TeV, using the ALICE detector at the LHC is reported. The measurement of the second-order Fourier coefficient of the particle azimuthal distribution, v2, is performed as a function of transverse momentum pT in the 0-20% high-multiplicity interval at both forward (2.03 < yCMS < 3.53) and backward (-4.46 < yCMS < -2.96) rapidities over a wide pT range, 0.5 < pT 10 GeV/c, in which a dominant contribution of muons from heavy-flavour hadron decays is expected at pT 2 GeV/c. The v2 coefficient of inclusive muons is extracted using two different techniques, namely two-particle cumulants, used for the first time for heavy-flavour measurements, and forward-central two-particle correlations. Both techniques give compatible results. A positive v2 is measured at both forward and backward rapidities with a significance larger than 4.7<sigma> and 7.6 sigma, respectively, in the interval 2 < pT < 6 GeV/c. Comparisons with previous measurements in p-Pb collisions at root sNN = 5.02 TeV, and with AMPT and CGC-based theoretical calculations are discussed. The findings impose new constraints on the theoretical interpretations of the origin of the collective behaviour in small collision systems. (c) 2023 European Organization for Nuclear Research. Published by Elsevier B.V. This is an open access article under the CC BY license (http:// creativecommons .org /licenses /by /4 .0/). Funded by SCOAP3.

PHYSICS LETTERS B 846, 137782, 2023. DOI: 10.1016/j.physletb.2023.137782

[P355-2023] "Measurements of the azimuthal anisotropy of prompt and nonprompt charmonia in PbPb collisions at √sNN=5.02 TeV"

Tumasyan, A.; Adam, W.; **Chinellato, J. A.*;** et al.
CMS Collaboration

The second-order (v(2)) and third-order (v(3)) Fourier coefficients describing the azimuthal anisotropy of prompt and nonprompt (from b-hadron decays) J/psi, as well as prompt psi(2S) mesons are measured in lead-lead collisions at a center-of-mass energy per nucleon pair of root s(NN) = 5.02TeV. The analysis uses a data set corresponding to an integrated luminosity of 1.61 nb(-1) recorded with the CMS detector. The J/psi and psi(2S) mesons are reconstructed using their dimuon decay channel. The v(2) and v(3) coefficients are extracted using the scalar product method and studied as functions of meson transverse momentum and collision centrality. The measured v(2) values for prompt J/psi mesons are found to be larger than those for nonprompt J/psi mesons. The prompt J/psi v(2) values at high pT are found to be underpredicted by a model incorporating only parton energy loss effects in a quark-gluon plasma medium. Prompt and nonprompt J/psi meson v(3) and prompt psi(2S) v(2) and v(3) values are also reported for the first time, providing new information about heavy quark interactions in the hot and dense medium created in heavy ion collisions.

JOURNAL OF HIGH ENERGY PHYSICS [10], 115, 2023. DOI: 10.1007/JHEP10(2023)115

[P356-2023] "Measurements of the Higgs boson production cross section and couplings in the W boson pair decay channel in proton-proton collisions at √s = 13 TeV"

Tumasyan, A.; Adam, W.; **Chinellato, J. A.*;** et al.
CMS Collaboration

Production cross sections of the standard model Higgs boson decaying to a pair of W bosons are measured in proton--proton collisions at a center-of-mass energy of 13 TeV. The analysis targets Higgs bosons produced via gluon fusion, vector boson fusion, and in association with a W or Z boson. Candidate events are required to have at least two charged leptons and moderate missing transverse momentum, targeting events with at least one leptonically decaying W boson originating from the Higgs boson. Results are presented in the form of inclusive and differential cross sections in the simplified template cross section framework, as well as couplings of the Higgs boson to vector bosons and fermions. The data set collected by the CMS detector during 2016-2018 is used, corresponding to an integrated luminosity of 138fb(-1). The signal strength modifier mu, defined as the ratio of the observed production rate in a given decay channel to the standard model expectation, is measured to be mu=0.95(-0.09)(+0.10). All results are found to be compatible with the standard model within the uncertainties.

EUROPEAN PHYSICAL JOURNAL C 83[7], 667, 2023. DOI: 10.1140/epjc/s10052-023-11632-6

[P357-2023] "Multi-pollutant biosorption of organic and inorganic pollutants by brown algae waste from alginate production: batch and fixed-bed investigation"

Nascimento Jr., W. J. do; Aguiar, G. H. de; Massarelli, R. C.; **Landers, R.***; Vieira, M. G. A.; Motta Sobrinho, M. A. da

The reuse of biomass waste has been gaining attention in adsorption processes to remove pollutants of emerging concern from water and wastewater. In this work, the potential of alginate-extracted macro-algae waste to uptake synthetic dyes and metal cations was evaluated in comparison with raw algae. In affinity assays, both materials were able to remove metal cations and cationic dyes up to maximum rates, and no significant removal was observed for an anionic dye in an acidic medium. Competition was observed in multi-component systems of metal cations and dyes. For binary samples containing organic and inorganic contaminants, kinetic modeling evidenced the distinct nature of both types of adsorbates. Pb(II) biosorption was best described as a first-order process, while second-order and Elovich models better fitted methyl blue (MB) uptake data. For equimolar binary samples, the Sips isothermal model fitted the experimental data more satisfactorily at room temperature. Isotherms for 20, 30, 40, and 60 degrees C exhibited favorable adsorption profiles with spontaneous Delta G values for both raw macro-algae and waste from alginate extraction. Maximum adsorption capacities were competitive with previous reports in the literature for a wide range of biomaterials, pointing to the slightly higher efficiency with algae waste in batch experiments. In elution tests, HNO3 (0.5 M) showed the best recovery rates of metal cations. Continuous biosorption operation revealed the performance of the brown algae waste was considerably more efficient than raw algae with breakthrough biosorption capacities up to 3.96 and 0.97 mmol.g-1 for the removal of Pb(II) and MB, respectively. A total of 3.0 g of algae and algae waste were able to deliver 1.20 and 1.62 L of contaminant-free water, respectively. XPS analyses corroborate previous assays that pointed to the prevalence of physisorption with evidence of complexation, ionic exchange, and hydrogen displacement mechanisms.

ENVIRONMENTAL SCIENCE AND POLLUTION RESEARCH, 2023. DOI: 10.1007/s11356-023-30511-x **Early Access Date: NOV 2023**

[P358-2023] "Multiplicity and rapidity dependence of K*(892)0 and φ(1020) production in p-Pb collisions at √sNN=5.02 TeV"

Acharya, S.; Adamová, D.; **Chinellato, D. D.*; Guardiano, G. G.*; Jahnke, C.*; Takahashi, J,*;** et al.
ALICE Collaboration

The transverse-momentum (p(T)) spectra of K* (892)(0) and phi(1020) measured with the ALICE detector up to p(T) = 16 GeV/c in the rapidity range -1.2 < y < 0.3, in p-Pb collisions at the center-of-mass energy per nucleon-nucleon collision root s(NN) = 5.02 TeV are presented as a function of charged particle multiplicity and rapidity. The measured p(T) distributions show a dependence on both multiplicity and rapidity at low p(T) whereas no significant dependence is observed at high p(T). A rapidity dependence is observed in the p(T)-integrated yield (dN/dy), whereas the mean transverse momentum (< pT >) shows a flat behavior as a function of rapidity. The rapidity asymmetry (Y-asym) at low p(T) (< 5 GeV/c) is more significant for higher multiplicity classes. At high p(T), no significant rapidity asymmetry is observed in any of the multiplicity classes. Both K* (892)(0) and phi(1020) showsimilar Y-asym. The nuclear modification factor (QCP) as a function of p(T) shows a Cronin-like enhancement at intermediate p(T), which is more prominent at higher rapidities (Pb-going direction) and in higher multiplicity classes. At high p(T) (> 5 GeV/c), the Q(CP) values are greater than unity and no significant rapidity dependence is observed.

EUROPEAN PHYSICAL JOURNAL C 83[6], 540, 2023. DOI: 10.1140/epjc/s10052-023-11449-3

[P359-2023] "Multiscale Monte Carlo simulations for dosimetry in x-ray breast imaging: Part I - Macroscopic scales"

Massera, R. T.*; Tomal, A.*; Thomson, R. M.

BackgroundX-ray breast imaging modalities are commonly employed for breast cancer detection, from screening programs to diagnosis. Thus, dosimetry studies are important for quality control and risk estimation since ionizing radiation is used.PurposeTo perform multiscale dosimetry assessments for different breast imaging modalities and for a variety of breast sizes and compositions. The first part of our study is focused on macroscopic scales (down to millimeters).MethodsNine anthropomorphic breast phantoms with a voxel resolution of 0.5 mm were computationally generated using the BreastPhantom software, representing three breast sizes with three distinct values of volume glandular fraction (VGF) for each size. Four breast imaging modalities were studied: digital mammography (DM), contrast-enhanced digital mammography (CEDM), digital breast tomosynthesis (DBT) and dedicated breast computed tomography (BCT). Additionally, the impact of tissue elemental compositions from two databases were compared. Monte Carlo (MC) simulations were performed with the MC-GPU code to obtain the 3D glandular dose distribution (GDD) for each case considered with the mean glandular dose (MGD) fixed at 4 mGy (to facilitate comparisons). ResultsThe GDD within the breast is more uniform for CEDM and BCT compared to DM and DBT. For large breasts and high VGF, the ratio between the minimum/maximum glandular dose to MGD is 0.12/4.02 for DM and 0.46/1.77 for BCT; the corresponding results for a small breast and low VGF are 0.35/1.98 (DM) and 0.63/1.42 (BCT). The elemental compositions of skin, adipose and glandular tissue have a considerable impact on the MGD, with variations up to 30% compared to the baseline. The inclusion of tissues other than glandular and adipose within the breast has a minor impact on MGD, with differences below 2%. Variations in the final compressed breast thickness alter the shape of the GDD, with a higher compression resulting in a more uniform GDD.ConclusionsFor a constant MGD, the GDD varies with imaging modality and breast compression. Elemental tissue compositions are an important factor for obtaining MGD values, being a source of systematic uncertainties in MC simulations and, consequently, in breast dosimetry.

MEDICAL PHYSICS,2023. DOI: 10.1002/mp.16910 **Early Access Date: DEC 2023**

[P360-2023] "Multiscale Monte Carlo simulations for dosimetry in x-ray breast imaging: Part II - Microscopic scales"

Massera, R. T.*; Tomal, A.*; Thomson, R. M.

BackgroundAlthough the benefits of breast screening and early diagnosis are known for reducing breast cancer mortality rates, the effects and risks of low radiation doses to the cells in the breast are still ongoing topics of study.PurposeTo study specific energy distributions (f(z,Dg)$f(z,D_{g})$) in cytoplasm and nuclei of cells corresponding to glandular tissue for different x-ray breast imaging modalities.MethodsA cubic lattice (500 mu m length side) containing 4064 spherical cells was irradiated with photons loaded from phase space files with varying glandular voxel doses (DgD_{g}). Specific energy distributions were scored for nucleus and cytoplasm compartments using the PENELOPE (v. 2018) + penEasy (v. 2020) Monte Carlo (MC) code. The phase space files, generated in part I of this work, were obtained from MC simulations in a voxelized anthropomorphic phantom corresponding to glandular voxels for different breast imaging modalities, including digital mammography (DM), digital breast tomosynthesis (DBT), contrast enhanced digital mammography (CEDM) and breast CT (BCT). ResultsIn general, the average specific energy in nuclei is higher than the respective glandular dose scored in the same region, by up to 10%. The specific energy distributions for nucleus and cytoplasm are directly related to the magnitude of the glandular dose in the voxel (DgD_{g}), with little dependence on the spatial location. For similar DgD_{g} values, f(z,Dg)$f(z,D_{g})$ for nuclei is different between DM/DBT and CEDM/BCT, indicating that distinct x-ray spectra play significant roles in f(z,Dg)$f(z,D_{g})$. In addition, this behavior is also present when the specific energy distribution (Fg(z)$F_{g}(z)$) is considered taking into account the GDD in the breast. ConclusionsMicrodosimetry studies are complementary to the traditional macroscopic breast dosimetry based on the mean glandular dose (MGD). For the same MGD, the specific energy distribution in glandular tissue varies between breast imaging modalities, indicating that this effect could be considered for studying the risks of exposing the breast to ionizing radiation.

MEDICAL PHYSICS, 2023. DOI: 10.1002/mp.16912 **Early Access Date: DEC 2023**

[P361-2023] "Nanomechanical Behavior of Pentagraphyne--Based Single-Layer and Nanotubes through Reactive Classical Molecular Dynamics"

Sousa, J. M. de*; Brandao, W. H. da S.; Silva, W. L. A. P.; Ribeiro Jr., L. A.; **Galvao, D. S.*;** Pereira Junior, M. L.

A novel 2D carbon allotrope, pentagraphyne (PG-yne), was introduced in a recent theoretical study. This unique structure is derived from pentagraphene by incorporating acetylenic linkages between sp3 and sp2 hybridized carbon atoms. Given its intriguing electronic and structural properties, it is imperative to investigate the mechanical characteristics and thermal responses of PG-yne in both monolayer and nanotube configurations, which encompass different chiralities and diameters. We conducted fully atomistic reactive molecular dynamics (MD) simulations employing the ReaxFF potential to address these aspects. Our findings reveal that Young's modulus of PG-yne monolayers stands at approximately 51 GPa at room temperature. In contrast, for the studied nanotubes, regardless of their chirality, it hovers around 45 GPa. Furthermore, our observations indicate that PG-yne-based systems feature an extensive and relatively flat plastic region before reaching the point of total fracture, irrespective of their topology. Regarding their thermal properties, we identified a melting point at approximately 3600 K, accompanied by a phase transition around 1100 K.

C-JOURNAL OF CARBON RESEARCH 9[4], 110, 2023. DOI: 10.3390/c9040110

[P362-2023] "Niobium and carbon nanostructured coatings for corrosion protection of the 316L stainless steel"

Ferreira, M. O. A.; Mariani, F. E.; Leite, N. B.; Gelamo, R. V.; Aoki, I. V.; **Siervo, A. de***; Pinto, H. C.; Moreto, J. A.

This work aims to investigate the influence of niobium and carbon nanostructured coatings on the corrosion resistance of the 316L SS. The coated and uncoated specimens were morphologically and structurally characterized by using OM, SEM/EDX, DRX, FTIR, Raman spectroscopy and XPS techniques. The corrosion behaviour was assessed by OCP, PPc, EIS as well as immersion tests in 0.6 mol L-1 NaCl solution. In addition, the average contact angles were used to evaluate the surfaces free energy by the Van Oss interfacial tension component theory approach. Results showed that the surface treatments positively influenced the corrosion resistance of the 316L SS and the coatings act as a protective barrier against corrosion process. The reactive sputtering technique increased the wettability of the surfaces in relation to the base material. Considering applications in aggressive media, the 316L SS/Nb2O5 specimen exhibits superior performance when compared to the base material and 316L SS/carbon.

MATERIALS CHEMISTRY AND PHYSICS 312, 128610, 2023. DOI: 10.1016/j.matchemphys.2023.128610

[P363-2023] "Observation of Same-Sign WW<Production from Double Parton Scattering in Proton-Proton Collisions at √s=13 TeV"

Tumasyan, A.; Adam, W.; **Chinellato, J. A.***; et al.
CMS Collaboration

The first observation of the production of (WW +/-)-W-+/- bosons from double parton scattering processes using same-sign electron-muon and dimuon events in proton-proton collisions is reported. The data sample corresponds to an integrated luminosity of 138 fb(-1) recorded at a center-of-mass energy of 13 TeV using the CMS detector at the CERN LHC. Multivariate discriminants are used to distinguish the signal process from the main backgrounds. A binned maximum likelihood fit is performed to extract the signal cross section. The measured cross section for production of same-sign W bosons decaying leptonically is 80.7 +/- 11.2(stat) (+9.5)(-8.6)(syst) +/- 12.1(model) fb, whereas the measured fiducial cross section is 6.28 +/- 0.81(stat) +/- 0.69(syst) +/- 0.37(model) fb. The observed significance of the signal is 6.2 standard deviations above the background-only hypothesis.

PHYSICAL REVIEW LETTERS 131[9], 091803, 2023. DOI: 10.1103/PhysRevLett.131.091803

[P364-2023] "Observation of the Rare Decay of the η Meson to Four Muons"

Hayrapetyan, A.; Tumasyan, A.; **Chinellato, J. A.*;** et al.
CMS Collaboration

A search for the rare eta -> mu(+)mu(-)mu(+)mu(-) double-Dalitz decay is performed using a sample of proton-proton collisions, collected by the CMS experiment at the CERN LHC with high-rate muon triggers during 2017 and 2018 and corresponding to an integrated luminosity of 101 fb(-1). A signal having a statistical significance well in excess of 5 standard deviations is observed. Using the eta -> mu(+)mu(-) decay as normalization, the branching fraction B(eta -> mu(+)mu(-)mu(+)mu(-)) = [5.0 +/- 0.8(stat) +/- 0.7(syst) +/- 0.7(B-2 mu)] x 10(-9) is measured, where the last term is the uncertainty in the normalization channel branching fraction. This work achieves an improved precision of over 5 orders of magnitude compared to previous results, leading to the first measurement of this branching fraction, which is found to agree with theoretical predictions.

PHYSICAL REVIEW LETTERS 131[9], 091903, 2023. DOI: 10.1103/PhysRevLett.131.091903

[P365-2023] "Observation of τ Lepton Pair Production in Ultraperipheral Pb-Pb Collisions at √sNN=5.02 TeV"

Tumasyan, A.; Adam, W.; **Chinellato, J A.***; et al.

We present an observation of photon-photon production of t lepton pairs in ultraperipheral lead-lead collisions. The measurement is based on a data sample with an integrated luminosity of 404 mu b(-1) collected by the CMS experiment at a center-of-mass energy per nucleon pair of root s(NN) = 5.02 TeV. The gamma gamma -> tau(+)tau(-) process is observed for tau(+)tau(-) events with a muon and three charged hadrons in the final state. The measured fiducial cross section is sigma(gamma gamma ->tau(+)tau(-)) = 4.8 +/- 0.6(stat) +/- 0.5(syst) mu b, where the second (third) term corresponds to the statistical (systematic) uncertainty in sigma(gamma gamma ->tau(+)tau(-)) in agreement with leading-order QED predictions. Using sigma(gamma gamma ->tau(+)tau(-)), we estimate a model-dependent value of the anomalous magnetic moment of the t lepton of at a(tau) = 0.001(-0.089)(+0.055).

PHYSICAL REVIEW LETTERS 131[15], 151803, 2023. DOI: 10.1103/PhysRevLett.131.151803

[P366-2023] "Outdoor systems performance and upgrade"

Lopes, L.; Andringa, S.; Assis, P.; **Dobrigkeit, C.***; et al.

Over the last two decades, the possibility of using RPCs in outdoors systems has increased considerably. Our group has participated in this effort by installing several systems and continues to work on their optimization, while simultaneously studying and developing new approaches that can use RPCs in outdoor applications.In particular, four detectors were deployed in the field at the Pierre Auger Observatory in 2019 remained inactive, awaiting the commissioning of support systems. During the pandemic the detectors were left without gas flow for more than two years, but were recently reactivated with no major problems.The LouMu project combines particle physics and geophysics in order to map meter-scale geologic structures, using Muon Tomography. Transmission muography is sensitive to the total amount of matter crossed by the muons, allowing to separate targets of different densities. In this exploratory project, it serves to identify unconsolidated rock zones, like geological faults and ore masses around an old Pyrite mine, now converted into a science center. The general goal is to compare how effective is the muographic survey when compared with the more standard geophysical techniques. The development of the RPC system used and the data from the last two years will be presented.Finally, recent advances in a large area (1 m2) double gap-sealed RPC will be presented.

NUCLEAR INSTRUMENTS & METHODS IN PHYSICS RESEARCH SECTION A-ACCELERATORS SPECTROMETERS DETECTORS AND ASSOCIATED EQUIPMENT 1054, 168446, 2023. DOI: 10.1016/j.nima.2023.168446

[P367-2023] "Performance of the local reconstruction algorithms for the CMS hadron calorimeter with Run 2 data"

Tumasyan, A.; Adam, W.; **Chinellato, J. A.***; et al.
CMS Collaboration

A description is presented of the algorithms used to reconstruct energy deposited in the CMS hadron calorimeter during Run 2 (2015-2018) of the LHC. During Run 2, the characteristic bunch-crossing spacing for proton-proton collisions was 25 ns,

which resulted in overlapping signals from adjacent crossings. The energy corresponding to a particular bunch crossing of interest is estimated using the known pulse shapes of energy depositions in the calorimeter, which are measured as functions of both energy and time. A variety of algorithms were developed to mitigate the effects of adjacent bunch crossings on local energy reconstruction in the hadron calorimeter in Run 2, and their performance is compared.

JOURNAL OF INSTRUMENTATION 18[11], P11017, 2023. DOI: 10.1088/1748-0221/18/11/P11017

[P368-2023] "Planar degeneracy of the three-gluon vertex"

Aguilar, A. C.*; Ferreira, M. N.; Papavassiliou, J.; **Santos, L. R.***

We present a detailed exploration of certain outstanding features of the transversely-projected three-gluon vertex, using the corresponding Schwinger-Dyson equation in conjunction with key results obtained from quenched lattice simulations. The main goal of this study is the scrutiny of the approximate property denominated "planar degeneracy", unveiled when the Bose symmetry of the vertex is properly exploited. The planar degeneracy leads to a particularly simple parametrization of the vertex, reducing its kinematic dependence to essentially a single variable. Our analysis, carried out in the absence of dynamical quarks, reveals that the planar degeneracy is particularly accurate for the description of the form factor associated with the classical tensor, for a wide array of arbitrary kinematic configurations. Instead, the remaining three form factors display considerable violations of this property. In addition, and in close connection with the previous point, we demonstrate the numerical dominance of the classical form factor over all others, except in the vicinity of the soft-gluon kinematics. The final upshot of these considerations is the emergence of a very compact description for the three--gluon vertex in general kinematics, which may simplify significantly nonperturbative applications involving this vertex.

EUROPEAN PHYSICAL JOURNAL C 83[6], 549,2023. DOI: 10.1140/epjc/s10052-023-11732-3

[P369-2023] "Pseudorapidity densities of charged particles with transverse momentum thresholds in pp collisions at √s=5.02 and 13 TeV"

Acharya, S.; Adamova, D.; **Chinellato, D. D.*; Guardiano, G. G.*; Jahnke, C.*; Takahashi, J.***; et al.
ALICE Collaboration

The pseudorapidity density of charged particles with minimum transverse momentum (p(T)) thresholds of 0.15, 0.5, 1, and 2 GeV/c is measured in pp collisions at the center of mass energies of root s = 5.02 and 13 TeV with the ALICE detector. The study is carried out for inelastic collisions with at least one primary charged particle having a pseudorapidity (eta) within +/- 0.8 and p(T) larger than the corresponding threshold. In addition, measurements without p(T)-thresholds are performed for inelastic and nonsingle-diffractive events as well as for inelastic events with at least one charged particle having vertical bar eta vertical bar < 1 in pp collisions at root s = 5.02 TeV for the first time at the LHC. These measurements are compared to the PYTHIA 6, PYTHIA 8, and EPOS-LHC models. In general, the models describe the eta dependence of particle production well. However, discrepancies are observed for the highest transverse momentum threshold (p(T) > 2 GeV/c), highlighting the importance of such measurements for tuning event generators. The new measurements agree within uncertainties with results from the ATLAS and CMS experiments obtained at root s = 13 TeV.

PHYSICAL REVIEW D 108[7], 072008, 2023. DOI: 10.1103/PhysRevD.108.072008

[P370-2023] "Reconstruction of decays to merged photons using end-to-end deep learning with domain continuation in the CMS detector"

Tumasyan, A.; Adam, W.; **Chinellato, J. A.***; et al.
CMS Collaboration

A novel technique based on machine learning is introduced to reconstruct the decays of highly Lorentz boosted particles. Using an end-to-end deep learning strategy, the technique bypasses existing rule-based particle reconstruction methods typically used in high energy physics analyses. It uses minimally processed detector data as input and directly outputs particle properties of interest. The new technique is demonstrated for the reconstruction of the invariant mass of particles decaying in the CMS detector. The decay of a hypothetical scalar particle A into two photons, A gamma gamma, is chosen as a benchmark decay. Lorentz boosts gamma L 1/4 60-600 are considered, ranging from regimes where both photons are resolved to those where the photons are closely merged as one object. A training method using domain continuation is introduced, enabling the invariant mass reconstruction of unresolved photon pairs in a novel way. The new technique is validated using pi 0 gamma gamma decays in LHC collision data.

PHYSICAL REVIEW D 108[5], 052002, 2023. DOI: 10.1103/PhysRevD.108.052002

[P371-2023] "Schwinger poles of the three-gluon vertex: symmetry and dynamics"

Aguilar, A. C.*; Ferreira, M. N.; **Oliveira, B. M.*;** Papavassiliou, J.; **Santos, L. R.***

The implementation of the Schwinger mechanism endows gluons with a nonperturbative mass through the formation of special massless poles in the fundamental QCD vertices; due to their longitudinal character, these poles do not cause divergences in on-shell amplitudes, but induce detectable effects in the Green's functions of the theory. Particularly important in this theoretical setup is the three-gluon vertex, whose pole content extends beyond the minimal structure required for the generation of a gluon mass. In the present work we analyze these additional pole patterns by means of two distinct, but ultimately equivalent, methods: the Slavnov-Taylor identity satisfied by the three-gluon vertex, and the nonlinear Schwinger-Dyson equation that governs the dynamical evolution of this vertex. Our analysis reveals that the Slavnov-Taylor identity imposes strict model-independent constraints on the associated residues, preventing them from vanishing. Approximate versions of these constraints are subsequently recovered from the Schwinger-Dyson equation, once the elements responsible for the activation of the Schwinger mechanism have been duly incorporated. The excellent coincidence between the two approaches exposes a profound connection between symmetry and dynamics, and serves as a nontrivial self--consistency test of this particular mass generating scenario.

EUROPEAN PHYSICAL JOURNAL C 83[10], 889, 2023. DOI: 10.1140/epjc/s10052-023-12058-w

[P372-2023] "Search for Exotic Higgs Boson Decays H -- AA -- 4γ with Events Containing Two Merged Diphotons in Proton-Proton Collisions at Vs=13 TeV"

Tumasyan, A.; Adam, W.; **Chinellato, J. A.***; et al.

We present the first direct search for exotic Higgs boson decays H -> AA, A -> gamma gamma in events with two photonlike objects. The hypothetical particle A is a low-mass spin-0 particle decaying promptly to a merged diphoton reconstructed as a single photonlike object.

We analyze the data collected by the CMS ffiffi experiment at V s = 13 TeV corresponding to an integrated luminosity of 136 fb-1. No excess above the estimated background is found. We set upper limits on the branching fraction B(H -> AA -> 4 gamma) of (0.9-3.3) x 10-3 at 95% confidence level for masses of A in the range 0.1-1.2 GeV.

PHYSICAL REVIEW LETTERS 131[10], 101801, 2023. DOI: 10.1103/PhysRevLett.131.101801

[P373-2023] "Search for pair-produced vector-like leptons in final states with third-generation leptons and at least three b quark jets in proton-proton collisions at √s=13 TeV"

Tumasyan, A.; Adam, W.; **Chinellato, J. A.***; et al.
CMS Collaboration

The first search is presented for vector-like leptons (VLLs) in the context of the "4321 model", an ultraviolet-complete model with the potential to explain existing B physics measurements that are in tension with standard model predictions. The analyzed data, corresponding to an integrated luminosity of 96.5 fb-1, were recorded in 2017 and 2018 with the CMS detector at the LHC in proton-proton collisions at root s = 13 TeV. Final states with >= 3 b-tagged jets and two third-generation leptons (tau tau, tau nu tau, or nu tau nu tau) are considered. Upper limits are derived on the VLL production cross section in the VLL mass range 500-1050 GeV. The maximum likelihood fit prefers the presence of signal at the level of 2.8 standard deviations, for a representative VLL mass point of 600 GeV. As a consequence, the observed upper limits are approximately double the expected limits.

PHYSICS LETTERS B 846, 137713, 2023. DOI: 10.1016/j.physletb.2023.137713

[P374-2023] "Search for the lepton-flavor violating decay of the Higgs boson and additional Higgs bosons in theeμ final state in proton-proton collisions at √s=13 TeV"

Hayrapetyan, A.; Tumasyan, A.; **Chinellato, J. A.***; et al.
CMS Collaboration

A search for the lepton-flavor violating decay of the Higgs boson and potential additional Higgs bosons with a mass in the range 110-160 GeV to an e(+/-)mu(-/+) pair is presented. The search is performed with a proton-proton collision dataset at a center-of-mass energy of 13 TeV collected by the CMS experiment at the LHC, corresponding to an integrated luminosity of 138 fb(-1). No excess is observed for the Higgs boson. The observed (expected) upper limit on the e(+/-)mu(-/+) branching fraction for it is determined to be 4.4(4.7) x 10(-5) at 95% confidence level, the most stringent limit set thus far from direct searches. The largest excess of events over the expected background in the full mass range of the search is observed at an e(+/-)mu(-/+) invariant mass of approximately 146 GeV with a local (global) significance of 3.8 (2.8) standard deviations.

PHYSICAL REVIEW D 108[7], 072004, 2023. DOI: 10.1103/PhysRevD.108.072004

[P375-2023] "Search for Z' bosons decaying to pairs of heavy Majorana neutrinos in proton-proton collisions at √s=13 TeV"

Tumasyan, A.; Adam, W.; **Chinellato, J. A.***; et al.
CMS Collaboration

A search for the production of pairs of heavy Majorana neutrinos (N-l) from the decays of Z' bosons is performed using the CMS detector at the LHC. The data were collected in proton--proton collisions at a center-of-mass energy of root s = 13TeV, with an integrated luminosity of 138 fb(-1). The signature for the search is an excess in the invariant mass distribution of the final-state objects, two same-flavor leptons (e or mu) and at least two jets. No significant excess of events beyond the expected background is observed. Upper limits at 95% confidence level are set on the product of the Z' production cross section and its branching fraction to a pair of N-l, as functions of N-l and Z' boson masses (m(Nl) land m(Z'), respectively) for m(Z') from 0.4 to 4.6TeV and m(Nl) from 0.1TeV to mZ'/2. In the theoretical framework of a left-right symmetric model, exclusion bounds in the m(Nl) - m(Z') plane are presented in both the electron and muon channels. The observed upper limit on m(Z') reaches up to 4.42TeV. These are the most restrictive limits to date on the mass of N-l as a function of the Z' boson mass.

JOURNAL OF HIGH ENERGY PHYSICS [11], 181, 2023. DOI: 10.1007/JHEP11(2023)181

[P376-2023] "Self-Healing E-tongue"

Riul Jr., A.*; Barros, A. de; **Gaál, G.*; Braunger, M. L.*; Jimenez, M. J.*;** Avila-Avendano, C.; **Rodrigues, V.*;** Andrade, M. J. de; Quevedo-Lopez, M.; **Alvarez, F.***; Baughman, R. H.

Self-healing materials inspire the next generation of multifunctional wearables and Internet of Things appliances. They expand the realm of thin film fabrication, enabling seamless conformational coverage irrespective of the shape complexity and surface geometry for electronic skins, smart textiles, soft robotics, and energy storage devices. Within this context, the layer-by-layer (LbL) technique is versatile for homogeneously dispersing materials onto various matrices. Moreover, it provides molecular level thickness control and coverage on practically any surface, with poly-(ethylenimine) (PEI) and poly--(acrylic acid) (PAA) being the most used materials primarily employed in self-healing LbL structures operating at room temperature. However, achieving thin film composites displaying controlled conductivity and healing ability is still challenging under ambient conditions. Here, PEI and PAA are mixed with conductive fillers (gold nanorods, poly-(3,4-ethylene dioxythiophene): polystyrenesulfonate (PEDOT:PSS), reduced graphene oxides, and multiwalled carbon nanotubes) in distinct LbL film architectures. Electrical (AC and DC), optical (Raman spectroscopy), and mechanical (nanoindentation) measurements are used for characterizing composite structures and properties. A delicate balance among electrical, mechanical, and structural characteristics must be accomplished for a controlled design of conductive self-healing composites. As a proof-of--concept, four LbL composites were chosen as sensing units in the first reported self-healing e-tongue. The sensor can easily distinguish basic tastes at low molar concentrations and differentiate trace levels of glucose in artificial sweat. The formed nanostructures enable smart coverages that have unique features for solving current technological challenges.

ACS APPLIED MATERIALS & INTERFACES 15[47], 55073-55081,2023. DOI: 10.1021/acsami.3c11590

[P377-2023] "Study of flavor dependence of the baryon-to--meson ratio in proton-proton collisions at √s=13 TeV"

Acharya, S.; Adamova, D.; **Chinellato, D. D.*; Guardiano, G. G.*; Jahnke, C.*; Liveraro, G. S. S.*; Takahashi, J.***; et al.

The production cross sections of D-0 and Lambda(+)(c) hadrons originating from beauty-hadron decays (i.e., nonprompt) were measured for the first time at midrapidity (|y| < 0.5)

by the ALICE Collaboration in proton-proton collisions at a center-of-mass energy root s = 13 TeV. They are described within uncertainties by perturbative QCD calculations employing the fragmentation fractions of beauty quarks to baryons measured at forward rapidity by the LHCb Collaboration. The bb production cross section per unit of rapidity at midrapidity, estimated from these measurements, is d sigma(bb)/dy|(|y|<0.5)= 83.1 +/- 3.5(stat) +/- 5.4(syst)(-3.2)(+12.3) (extrap) mu b. The baryon-to-meson ratios are computed to investigate the hadronization mechanism of beauty quarks. The nonprompt Lambda(+)(c)/D-0 production ratio has a similar trend to the one measured for the promptly produced charmed particles and to the p/pi(+) and Lambda/K-S(0) ratios, suggesting a similar baryon-formation mechanism among light, strange, charm, and beauty hadrons. The p(T) -integrated nonprompt Lambda(+)(c)/D-0 ratio is found to be significantly higher than the one measured in e(+)e(-) collisions.

PHYSICAL REVIEW D 108[11], 112003, 2023. DOI: 10.1103/PhysRevD.108.112003

[P378-2023] "Study of the p-p-K+ and p-p-K- dynamics using the femtoscopy technique"

Acharya, S.; Adamová, D.; **Chinellato, D. D.*; Guardiano, G. G.*; Jahnke, C.*; .; Liveraro, G. S. S.*; Takahashi, J,*;** et al. ALICE Collaboration

The interactions of kaons (K) and antikaons ((K) over bar) with few nucleons (N) were studied so far using kaonic atom data and measurements of kaon production and interaction yields in nuclei. Some details of the three-body KNN and KNN dynamics are still not well understood, mainly due to the overlap with multi-nucleon interactions in nuclei. An alternative method to probe the dynamics of three-body systems with kaons is to study the final state interaction within triplet of particles emitted in pp collisions at the Large Hadron Collider, which are free from effects due to the presence of bound nucleons. This Letter reports the first femtoscopic study of p-p-K+ and p-p-K- correlations measured in high-multiplicity pp collisions at root s = 13 TeV by the ALICE Collaboration. The analysis shows that the measured p-p-K+ and p-p-K- correlation functions can be interpreted in terms of pairwise interactions in the triplets, indicating that the dynamics of such systems is dominated by the two-body interactions without significant contributions from three-body effects or bound states.

EUROPEAN PHYSICAL JOURNAL A 59[12], 298, 2023. DOI: 10.1140/epja/s10050-023-01139-9

[P379-2023] "Synchronization of Sakaguchi swarmalators"

Lizarraga, J. U. F.*; Aguiar, M. A. M. de*

Swarmalators are phase oscillators that cluster in space, like fireflies flashing in a swarm to attract mates. Interactions between particles, which tend to synchronize their phases and align their motion, decrease with the distance and phase difference between them, coupling the spatial and phase dynamics. In this work, we explore the effects of inducing phase frustration on a system of swarmalators that move on a one-dimensional ring. Our model is inspired by the well-known Kuramoto-Sakaguchi equations. We find, numerically and analytically, the ordered and disordered states that emerge in the system. The active states, not present in the model without frustration, resemble states found previously in numerical studies for the two-dimensional swarmalators system. One of these states, in particular, shows similarities to turbulence generated in a flattened media. We show that all ordered states can be generated for any values of the coupling constants by tuning the phase frustration parameters only. Moreover, many of these combinations display multistability.

PHYSICAL REVIEW E 108[2], 024212, 2023. DOI: 10.1103/PhysRevE.108.024212

[P380-2023] "Synergy between deep neural networks and the variational Monte Carlo method for small 4HeN clusters"

Freitas, W.*; Vitiello, S.A.*

We introduce a neural network-based approach for modeling wave functions that satisfy Bose-Einstein statistics. Applying this ing from 2 to 14 atoms), we accurately predict ground state energies, pair density functions, and two-body contact parameters C(N) 2 related to weak unitarity. The results obtained via the variational Monte Carlo method exhibit remarkable agreement with previous studies using the diffusion Monte Carlo method, which is considered exact within its statistical uncertainties. This indicates the effectiveness of our neural network approach for investigating many-body systems governed by Bose-Einstein statistics.

QUANTUM, 2023. Early Access Date: DEC 2023

[P381-2023] "Terahertz Twistoptics-Engineering Canalized Phonon Polaritons"

Obst, M.; Nörenberg, T.; Alvarez-Pérez, G.; Oliveira, T.V.A.G. de; Taboada-Gutiérrez, J.; **Feres, F.H.***; Kaps, F.G.; Hatem, O.; Luferau, A.; Nikitin, A.Y.; Klopf, J.M.; Alonso-González, P.; Kehr, S.C.; Eng, L.M.

The terahertz (THz) frequency range is key to studying collective excitations in many crystals and organic molecules. However, due to the large wavelength of THz radiation, the local probing of these excitations in smaller crystalline structures or few-molecule arrangements requires sophisticated methods to confine THz light down to the nanometer length scale, as well as to manipulate such a confined radiation. For this purpose, in recent years, taking advantage of hyperbolic phonon polaritons (HPhPs) in highly anisotropic van der Waals (vdW) materials has emerged as a promising approach, offering a multitude of manipulation options, such as control over the wavefront shape and propagation direction. Here, we demonstrate the THz application of twist-angle-induced HPhP manipulation, designing the propagation of confined THz radiation between 8.39 and 8.98 THz in the vdW material alpha-molybdenum trioxide (alpha-MoO3), hence extending twistoptics to this intriguing frequency range. Our images, recorded by near-field optical microscopy, show the frequency- and twist-angle-dependent changes between hyperbolic and elliptic polariton propagation, revealing a polaritonic transition at THz frequencies. As a result, we are able to allocate canalization (highly collimated propagation) of confined THz radiation by carefully adjusting these two parameters, i.e. frequency and twist angle. Specifically, we report polariton canalization in alpha-MoO3 at 8.67 THz for a twist angle of 50 degrees. Our results demonstrate the precise control and manipulation of confined collective excitations at THz frequencies, particularly offering possibilities for nanophotonic applications.

ACS NANO 17[19], 19313-19322, 2023. DOI: 10.1021/acsnano.3c06477

[P382-2023] "The CYGNO experiment: a directional Dark Matter detector with optical readout"

Amaro, F. D.; Antonietti, R.; Baracchini, E.; **Kemp, E.***; et al.

We are going to discuss the R&D and the prospects for the CYGNO project, towards the development of an innovative, high precision 3D tracking Time Projection Chamber with optical readout using He:CF4 gas at 1 bar.

CYGNO uses a stack of triple thin GEMs for charge multiplication, this induces scintillation in CF4 gas, which is readout by PMTs and sCMOS cameras. High granularity and low readout noise of sCMOS along with high sampling of PMT allows CYGNO to have 3D tracking with head tail capability and particle identification down to O(keV) energy for directional Dark Matter searches and solar neutrino spectroscopy. We will present the most recent R&D results from the CYGNO project, and in particular the overground commissioning of the largest prototype developed so far, LIME with a 33x33 cm2 readout plane and 50 cm of drift length, for a total of 50 litres active volume. We will illustrate the LIME response characterisation between 3.7 keV and 44 keV by means of multiple X-ray sources, and the data Monte-Carlo comparison of simulated sCMOS images in this energy range. Furthermore, we will present current LIME installation, operation and data taking at underground Laboratori Nazionali del Gran Sasso (LNGS), serving as demonstrator for the development of a 0.4 m3 CYGNO detector. We will conclude by mentioning the technical choices and the prospects of the 0.4 m3 detector, as laid out in the Technical Design Report (TDR) recently produced by our collaboration.

JOURNAL OF INSTRUMENTATION 18[9], C09010, 2023. DOI: 10.1088/1748-0221/18/09/C09010

[P383-2023] "The response of 316 L steel manufactured by selective laser melting route to high-temperature oxidation behaviour: The role of microstructure modification"

Kumar, V.; Pruncu, C. I.; Wang, Y. P.; **Echeverrigaray, F. G.*; Alvarez, F.***; Perotti, B. L.; Figueroa, C. A.; Hosmani, S. S.

The current work examines the effect of 316 L steel's microstructure, which is modified through varying scanning angles with the sample surface (HNS (0 degrees), INS (45 degrees), and VNS (90 degrees)) in the selective laser melting (SLM) method and through surface mechanical attrition treatment (SMAT), on its high-temperature oxidation behaviour (at 600-800 degrees C) is investigated. We have obtained a deeper understanding of the steel's oxidation behaviour by applying various characterisation techniques. The SMATed steel has a -1000 mu m thick deformed layer containing a gradient microstructure, and its topmost layer contains fine twins and nanograins (-30 nm). The hardness of this surface is-1.65 times the non-treated steel's hardness. All samples follow a parabolic rate law during oxidation. The VNS sample unveils the slowest oxidation rate amid the non-treated samples. SMAT increases the activation energy of oxidation. The distribution of elements across the oxidised samples' cross-section shows discontinuous Cr spreading within the oxide layer on the non-treated samples; however, the deformed samples show uniform distribution. Unlike non-SMATed samples, a minute decline in Cr and Mn content is observed underneath the oxide layer on the SMATed samples, confirming their enhanced outward diffusion. The oxide layer on SMATed samples has more Cr-and Mn-rich oxides. These oxides occupy the grain boundaries of the oxidised non--SMATed surfaces, where the micro-pores and cracks are present. Conversely, oxidised SMATed surfaces display uniform, defect-free Cr-and Mn-rich oxides with finer grains. Moreover, the SMATed layer remains reasonably stable during high-temperature oxidation (hardness drop ranges between-9 and -30%).

MATERIALS CHARACTERIZATION 207, 113531, 2023. DOI: 10.1016/j.matchar.2023.113531

[P384-2023] "Tuning the Chemical and Electrochemical Properties of Paper-Based Carbon Electrodes by Pyrolysis of Polydopamine"

Rocha, J.F.; Oliveira, J.C. de; Bettini, J.; Strauss, M.; **Selmi, G.S.***; Okazaki, A.K.; **Oliveira, R.F. de***; Lima, R.S.; Santhiago, M.

Electrochemical paper-based analytical devices represent an important platform for portable, low-cost, affordable, and decentralized diagnostics. For this kind of application, chemical functionalization plays a pivotal role to ensure high clinical performance by tuning surface properties and the area of electrodes. However, controlling different surface properties of electrodes by using a single functionalization route is still challenging. In this work, we attempted to tune the wettability, chemical composition, and electroactive area of carbon-paper-based devices by thermally treating polydopamine (PDA) at different temperatures. PDA films were deposited onto pyrolyzed paper (PP) electrodes and thermally treated in the range of 300-1000 degrees C. After deposition of PDA, the surface is rich in nitrogen and oxygen, it is superhydrophilic, and it has a high electroactive area. As the temperature increases, the surface becomes hydrophobic, and the electroactive area decreases. The surface modifications were followed by Raman, X-ray photoelectron microscopy (XPS), laser scanning confocal microscopy (LSCM), contact angle, scanning electron microscopy (SEM-EDS), electrical measurements, transmission electron microscopy (TEM), and electrochemical experiments. In addition, the chemical composition of nitrogen species can be tuned on the surface. As a proof of concept, we employed PDA-treated surfaces to anchor [AuCl4](-) ions. After electrochemical reduction, we observed that it is possible to control the size of the nanoparticles on the surface. Our route opens a new avenue to add versatility to electrochemical interfaces in the field of paper-based electrochemical biosensors.

ACS MEASUREMENT SCIENCE AU, 20223. DOI: 10.1021/acsmeasuresciau.3c00063 **Early Access Date: DEC 2023**

[P385-2023] "Using a resource theoretic perspective to witness and engineer quantum generalized contextuality for prepare-and-measure scenarios"

Wagner, R.; **Baldijao, R. D.***; Tezzin, A.; Amaral, B.

We employ the resource theory of generalized contextuality as a tool for analyzing the structure of prepare-and-measure scenarios. We argue that this framework simplifies proofs of quantum contextuality in complex scenarios and strengthens existing arguments regarding robustness of experimental implementations. As a case study, we demonstrate quantum contextuality associated with any nontrivial noncontextuality inequality for a class of useful scenarios by noticing a connection between the resource theory and measurement simulability. Additionally, we expose a formal composition rule that allows engineering complex scenarios from simpler ones. This approach provides insights into the noncontextual polytope structure for complex scenarios and facilitates the identification of possible quantum violations of noncontextuality inequalities.

JOURNAL OF PHYSICS A-MATHEMATICAL AND THEORETICAL 56[50], 505303, 2023. DOI: 10.1088/1751-8121/ad0bcc

Eventos publicados 2023

[P386-2023] "Development of resistors with TaxNy deposited by RF sputtering using lithography technique"

Cesar, R. R.; **Mederos, M.***; Joanni, E.; Andrade, V. M.; Teixeira, R. C.; Diniz, J. A.
IEEE

In this work, a TaxNy thin film was used to manufacture resistors. The film was deposited by RF sputtering on an 96% polished alumina substrate, and it has a thickness, sheet resistance and resistivity of 150 nm, 181.63 Omega/sq and 2.72 m Omega cm, respectively.

Here, two types of resistor configurations were developed. The first one, is a set of resistors composed of five resistors with fixed length (L) and varying width (W) values. The second one is a set with TLM (Transfer Length Method) type configuration, which consists of six resistors in series with a fixed width (W) value and varying length (L) values. Both resistor configurations, shown a dependence almost linear with the resistance and a reproductive behavior, which allows uniformity in the manufacturing process. This study show that it is possible to use TaxNy films to manufacture resistors that permit you to tune the resistance values according to the needs of your application, for example in Multi-chip module (MCM).

37TH SYMPOSIUM ON MICROELECTRONICS TECHNOLOGY AND DEVICES, SBMICRO Book Series: Microelectronics Technology and Devices, 2023. DOI: 10.1109/SBMicro60499.2023.10302490

[P387-2023] "Sensing with agar-based optical waveguides"

Fujiwaraa, E.; **Cordeirob, C. M. B.***; Okuc, H.; Suzukia, C. K. Shaw J. A.; Matoba O.; Valenta C. R. (ed.)

The growing demand for biocompatible and biodegradable sensing devices emerges to fulfill applications in medicine, tissue engineering, and environmental monitoring. Nowadays, optical waveguides conceived with unconventional materials (like silk, cellulose, green polymers, and hydrogels) have replaced silica and polymer-based devices in optogenetics, phototherapy, and intra-body assessment. However, most biodegradable optical materials rely on expensive resources and intricate processing. Agar is an edible, soft, and renewable alternative presenting singular features: gelation at low temperatures, thermal reversibility, moldability, and transparency. Furthermore, one may enhance the optical and mechanical properties of the agar samples by choosing the chemical composition. This work proposes the design, characterization, and application of agar-based devices for optical sensing. Firstly, melt solutions comprising food-grade agar and water undergo solidification inside molds to create standard and structured optical fibers and waveguides. Besides, adding glycerol improves mechanical strength and stability, reduces optical losses, and provides reliable refractive index control. Subsequently, experiments evaluate the optic response of agar devices to mechanical, thermal, electrical, and chemical stimuli. Illumination with a visible laser creates speckle fields susceptible to mode coupling and phase deviation effects. Therefore, one may analyze these speckle patterns with image processing techniques to detect subtle changes in the output light and retrieve the measured parameters with high sensitivity through a straightforward camera-based setup. The agar optical waveguides provide new perspectives for physical and biochemical sensing based on an edible and biodegradable material for intra-body applications and environmental monitoring.

SPIE FUTURE SENSING TECHNOLOGIES 2023 Book Series: Proceedings of SPIE Volume: 12327 Article Number: 123270N,2023. DOI: 10.1117/12.2666266

Meeting abstract 2023

[Me001-2023] "A hierarchical approach for the use of functional near-infrared spectroscopy to interrogate residual cognitive function in the intensive care unit"

Kazazian, K.; Abdalmalak, A.; Norton, L.; Novi, S.; Moulavi-Ardakani, R.; Kolisnyk, M.; Gofton, T. E.; **Mesquita, R. C.*;** Owen, A.M.; Debicki, D.

BRAIN INJURY Meeting Abstract: 468, 37, 188-188, Supplement: 1, 2023

Artigos publicados 2024

[P001-2024] "3D-printed flexible energy harvesting devices designed using non-layered two-dimensional natural tourmaline silicates"

Mahapatra, P.L.; **Tromer, R.*;** Jayakumar, A.; Costin, G.; Lahiri, B.; Nair, R.R.; Roy, D.; Roy, A.K.; Pandey, P.; **Galvao, D.S.*;** Tiwary, C.S.

Sustainable energy solutions require high-performance and widely available materials, which could be easily engineered/scaled up to the required dimensions. Natural silicates, being environmentally stable and abundantly accessible, emerge as promising candidates for the development of energy devices. Here, we demonstrate the synthesis of two-dimensional (2D), non-layered tourmaline silicates (T-silicates) through an easily scalable liquid-phase exfoliation method. The 2D T-silicate is used to design fabric-based energy harvesting devices and cellulose-based 3D-printed structures for flexible electronics. The 2D T-silicate energy harvesting device, which is made of fabric, generates a voltage of approximately 10 V when it is tapped with a force of approximately 8.8 N at room temperature. At slightly higher temperatures, specifically at 50 degrees C, a small force of only 0.98 N can produce around 9.2 V. The 3D printed device with mesh design also produced similar to 3 V (peak to peak) upon tapping with a finger. The theoretically estimated piezoelectric coefficient was 4.3 x 10-10 C m-2, and the flexoelectric coefficient was 0.3 nC m-2. The study shows that ultrathin T-silicates can be used not only in fabrics but also in 3D printing for energy harvesting applications. This innovative work opens up new possibilities for sustainable energy solutions by combining advanced materials with state-of-the-art fabrication techniques. This paper shows how non-layered naturally occurring tourmaline silicates can be exfoliated into 2D structures for use in fabrics and 3D printed biomedical health monitoring devices.

JOURNAL OF MATERIALS CHEMISTRY C, 2024. DOI: 10.1039/d3tc04167k **Early Access Date: FEB 2024**

[P002-2024] "A procedure to minimize EEG variability for BCI applications"

Melo, G. C. de; **Castellano, G.***; Forner-Cordero, A.

A Brain-Computer Interface (BCI) decodes brain activities to translate them into computer commands. Electro-encephalography is the most widely adopted technique for brain signal recording in BCIs, because of practical and safety reasons. However, EEG signals show a significant intra-subject variability, which constitutes a major challenge for BCI development. The main goal of this work is to improve a pseudo-online movement detection system using motor imagery EEG signals that simulate the BCI input. We propose a strategy that aims at minimizing the effects of the poor spatial resolution and the active reference electrode based on finding the best combinations of electrode pairs. The proposed method finds subject-specific pairs of electrodes along with signal transformations that provide the more stable results. The average accuracy across 15 subjects was 95 %. It was also seen that energy signals in the delta band (0-4 Hz) of the electrode line CCP (according to the 10-20 system) are associated to the lowest variability. The hypothesis of lower variability being associated to movement related information and therefore to higher accuracy in classification was confirmed by the results. The main conclusion is that it is possible to overcome in some level the signal variability without introducing mathematical or physical uncertainties inherent to commonly adopted approaches such as spatial filters or volume conduction modeling, for instance. The contribution of this work is the procedure to minimize EEG variability for BCI applications.The significance is the possibility to apply the procedure to any set of channels and transformations.

BIOMEDICAL SIGNAL PROCESSING AND CONTROL 89, 105745, 2024. DOI: 10.1016/j.bspc.2023.105745

[P003-2024] "Adaptive foraging of pollinators fosters gradual tipping under resource competition and rapid environmental change"

Terpstra, S.; **Marquitti, F. M. D.***; Vasconcelos, V. V.

Plant and pollinator communities are vital for transnational food chains. Like many natural systems, they are affected by global change: rapidly deteriorating conditions threaten their numbers. Previous theoretical studies identified the potential for community-wide collapse above critical levels of environmental stressors-so-called bifurcation-induced tipping points. Fortunately, even as conditions deteriorate, individuals have some adaptive capacity, potentially increasing the boundary for a safe operating space where changes in ecological processes are reversible. Our study considers this adaptive capacity of pollinators to resource availability and identifies a new threat to disturbed pollinator communities. We model the adaptive foraging of pollinators in changing environments. Pollinator's adaptive foraging alters the dynamical responses of species, to the advantage of some-typically generalists-and the disadvantage of others, with systematic non-linear and non-monotonic effects on the abundance of particular species. We show that, in addition to the extent of environmental stress, the pace of change of environmental stress can also lead to the early collapse of both adaptive and nonadaptive pollinator communities. Specifically, perturbed communities exhibit rate-induced tipping points at stress levels within the safe boundary defined for constant stressors. With adaptive foraging, tipping is a more asynchronous collapse of species compared to nonadaptive pollinator communities, meaning that not all pollinator species reach a tipping event simultaneously. These results suggest that it is essential to consider the adaptive capacity of pollinator communities for monitoring and conservation. Both the extent and the rate of stress change relative to the ability of communities to recover are critical environmental boundaries. Plant and pollinator communities, which support global food chains, are threatened. A significant problem is the reduction of pollination, where not enough plants are pollinated and are at risk of becoming extinct. Environmental change, such as climate change or increasing pesticide use, can cause this reduction. As long as these changes stay under certain boundaries, undesirable ecological processes like the reduction in pollination are reversible. Crossing these boundaries means tipping of pollinator communities might occur; the system might collapse. Pollinator communities can adapt, for instance, through adaptive foraging by changing which plants they prefer in response to environmental deterioration. We include adaptive foraging in a theoretical model of plant and pollinator communities. We show that plant and pollinator communities are vulnerable to the extent of stressors but also to how fast these stressors increase. Our model shows that, with adaptation, the extinction of species is more sequential and spreads out in time and may even temporarily favor especially generalist species.

PLOS COMPUTATIONAL BIOLOGY 20[1], e1011762, 2024. DOI: 10.1371/journal.pcbi.1011762

[P004-2024] "Ballistic properties of highly stretchable graphene kirigami pyramid"

Moura, A.*; Ipaves, B.; **Galvao, D. S.***; Autreto, P. A. D.

Graphene kirigamis, characterized by patterned cuts, can enhance some of the graphene's mechanical and electronic properties. In this work, we report the first study of the mechanical and ballistic behavior of single and multi- layered graphene kirigami pyramid (GKP). We have carried out fully atomistic reactive molecular dynamics simulations. The GKP structures exhibit a large kinetic energy absorption capability due to their topology, which creates multi-step dissipation mechanisms that block crack propagation. Our results demonstrate that even having significantly less mass, GKP can outperform graphene structures of similar dimensions in terms of absorbing kinetic energy capabilities.

COMPUTATIONAL MATERIALS SCIENCE 232, 112558, 2024. DOI: 10.1016/j.commatsci.2023.112558

[P005-2024] "Biotene: Earth-Abundant 2D Material as Sustainable Anode for Li/Na-Ion Battery"

Pramanik, A.; Mahapatra, P. L.; **Tromer, R.***; Xu, J. N.; Costin, G.; Li, C. X.; Saju, S.; Alhashim, S.; Pandey, K.; Srivastava, A.; Vajtai, R.; **Galvao, D. S.***; Tiwary, C. S.; Ajayan, P. M.

Natural ores are abundant, cost-effective, and environmentally friendly. Ultrathin (2D) layers of a naturally abundant van der Waals mineral, Biotite, have been prepared in bulk via exfoliation. We report here that this 2D Biotene material has shown extraordinary Li-Na-ion battery anode properties with ultralong cycling stability. Biotene shows 302 and 141 mAh g(-1) first cycle-specific charge capacity for Li- and Na--ion battery applications with similar to 90% initial Coulombic efficiency. The electrode exhibits significantly extended cycling stability with similar to 75% capacity retention after 4000 cycles even at higher current densities (500-2000 mA g(-1)). Further, density functional theory studies show the possible Li intercalation mechanism between the 2D Biotene layers. Our work brings new directions toward designing the next generation of metal-ion battery anodes.

ACS APPLIED MATERIALS & INTERFACES 16[2], 2417-2427, 2024. DOI: 10.1021/acsami.3c15664

[P006-2024] "Computational prediction of high thermoelectric performance in As2Se3 by engineering out-of-equilibrium defects"

Chaves, A. S.; **Silva, M. A.*; Antonelli, A.***

We employed first-principles calculations to investigate the thermoelectric transport properties of the compound As2Se3. Early experiments and calculations have indicated that these properties are controlled by a kind of native defect called antisites. Our calculations using the linearized Boltzmann transport equation within the relaxation time approximation show good agreement with the experiments for defect concentrations of the order of 10(19) cm(-3). Based on our total energy calculations, we estimated the equilibrium concentration of antisite defects to be about 10(14) cm(-3). These results suggest that the large concentration of defects in the experiments is due to kinetic and/or off-stoichiometry effects and in principle it could be lowered, yielding relaxation times similar to those found in other chalcogenide compounds. In this case, for relaxation time higher than 10 fs, we obtained high thermoelectric figures of merit of 3 for the p-type material and 2 for the n-type one.

PHYSICAL CHEMISTRY CHEMICAL PHYSICS 26[5], 4144-4150, 2024. DOI: 10.1039/d3cp03629d

[P007-2024] "Disposable and eco-friendly electrochemical immunosensor for rapid detection of SARS-CoV-2"

Rocha, D. S.; Baldo, T. A.; Silva Neto, H. A.; Duarte Junior, G. F.; Bazílio, G. S.; Borges, C. L.; Parente Rocha, J. A.; Araujo, W. R. de; **Siervo, A. de***; Paixa, T. L. R. C.; Coltro, W. K. T.

This study describes the development of a simple, disposable, and eco-friendly electrochemical immunosensor for rapid detection of severe acute respiratory syndrome coronavirus 2 (SARS-CoV-2). Electrochemical devices were manufactured by stencil-printing using low-cost materials such as polyester sheets, graphite flakes, and natural resin. The immunosensor comprises gold nanoparticles stabilized with cysteamine, glutaraldehyde, anti-SARS-CoV-2 S protein monoclonal antibody (Ab1) as the biological receptor, and bovine serum albumin as a protec--tive layer. The COVID-19 diagnostic was based on rapid square wave voltammetry measurements (15 min) using [Fe(CN)6]3-/4- as a redox probe. The method presented a linear response in the concentration range from 250 pg mL-1 to 20 mu g mL-1 S protein, with a limit of detection of 36.3 pg mL-1. The proposed immunosensor was stable for up to two weeks when stored at 4 degrees C and it demonstrated excellent clinical performance in diagnosing COVID-19 when applied to a panel of 44 undiluted swab samples collected from symptomatic patients. In comparison with results obtained through the quantitative reverse transcription polymerase chain reaction method, the proposed immunosensor offered 100 % accuracy, thus emerging as a powerful alternative candidate for routine and decentralized testing, which can be helpful in controlling the COVID-19 outbreak.

TALANTA 268, 25337, 2024. DOI: 10.1016/j.talanta.2023.125337

[P008-2024] "Evolution of cooperation in a two-species system with a common resource pool"

Salles, L. F. P.*; Aguiar, M. A. M. de*; Marquitti, F. M. D.*

Understanding the evolution of cooperation is a major question in Evolutionary Biology. Here, we extend a previously proposed mathematical model in Evolutionary Game Theory that investigated how resource use by a single species composed of cooperators and defectors may lead to its maintenance or extinction. We include another species in the model, so as to investigate how different intra and interspecific interactions of cooperative or competitive nature among individuals that share the same essential resource may drive the survival and evolution of the species. Several outcomes emerge from the model, depending on the configuration of the payoff matrix, the individual contribution to the resource pool, the competition intensity between species, and the initial conditions of the system dynamics. Observed results include scenarios in which species thrive due to the action of cooperators, but also scenarios in which both species collapse due to lack of cooperation and, consequently, of resources. In particular, a high initial availability of resources may be the determinant factor to the survival of both species. Interestingly, cooperation may be more favored when individuals have less incentive to cooperate with others, and the survival of their populations may depend crucially on their competitive capacities.

JOURNAL OF THEORETICAL BIOLOGY 577, 111670, 2024. DOI: 10.1016/j.jtbi.2023.111670

[P009-2024] "Hydrogen atom/molecule adsorption on 2D metallic porphyrin: A first-principles study"

Tromer, R. M.*; Felix, I. M.; **Felix, L. C.***; Machado, L. D.; Woellner, C. F.; **Galvao, D. S.***

Hydrogen is a promising element for applications in new energy sources like fuel cells. One key issue for such applications is storing hydrogen. And, to improve storage capacity, understanding the interaction mechanism between hydrogen and possible storage materials is critical. This work uses DFT simulations to comprehensively investigate the adsorption mechanism of H/H2 on the 2D metallic porphyrins with one transition metal in its center.Our results suggest that the mechanism for adsorption of H (H2) is chemisorption (physisorption). The maximum adsorption energy for atomic hydrogen was -3.7 eV for 2D porphyrins embedded with vanadium or chromium atoms. Our results also revealed charge transfer of up -0.43 e to chemisorbed H atoms. In contrast, the maximum adsorption energy calculated for molecular hydrogen was -122.5 meV for 2D porphyrins embedded with scandium atoms. Furthermore, charge transfer was minimal for physisorption. Finally, we also determined that uniaxial strain has a minimal effect on the adsorption properties of 2D metallic porphyrins.

CHEMICAL PHYSICS 577, 112142, 2024. DOI: 10.1016/j.chemphys.2023.112142

[P010-2024] "Investigation of protein-protein interactions and hotspot region on the NSP7-NSP8 binding site in NSP12 of SARS-CoV-2"

Lima Neto, J. X.; Bezerra, K. S.; Barbosa, E. D.; Araujo, R. L.; **Galvao, D. S.***; Lyra, M. L.; Oliveira, J. I. N.; Akash, S.; Bin Jardan, Y. A.; Nafidi, H. A.; Bourhia, M.; Fulco, U. L.

Background: The RNA-dependent RNA polymerase (RdRp) complex, essential in viral transcription and replication, is a key target for antiviral therapeutics. The core unit of RdRp comprises the nonstructural protein NSP12, with NSP7 and two copies of NSP8 (NSP81 and NSP82) binding to NSP12 to enhance its affinity for viral RNA and polymerase activity. Notably, the interfaces between these subunits are highly conserved, simplifying the design of molecules that can disrupt their interaction.Methods: We conducted a detailed quantum biochemical analysis to characterize the interactions within the NSP12--NSP7, NSP12-NSP81, and NSP12-NSP82 dimers. Our objective was to ascertain the contribution of individual amino acids to these protein-protein interactions, pinpointing hotspot regions crucial for complex stability.Results: The analysis revealed that the NSP12-NSP81 complex possessed the highest total interaction energy (TIE), with 14 pairs of residues demonstrating significant energetic contributions. In contrast, the NSP12--NSP7 complex exhibited substantial interactions in 8 residue pairs, while the NSP12-NSP82 complex had only one pair showing notable interaction. The study highlighted the importance of hydrogen bonds and pi-alkyl interactions in maintaining these complexes. Intriguingly, introducing the RNA sequence with Remdesivir into the complex resulted in negligible alterations in both interaction energy and geometric configuration. Conclusion: Our comprehensive analysis of the RdRp complex at the protein-protein interface provides invaluable insights into interaction dynamics and energetics. These findings can guide the design of small molecules or peptide/peptidomimetic ligands to disrupt these critical interactions, offering a strategic pathway for developing effective antiviral drugs.

FRONTIERS IN MOLECULAR BIOSCIENCES 10, 1325588, 2024. DOI: 10.3389/fmolb.2023.1325588

[P011-2024] "Niobium and carbon nanostructured coatings for corrosion protection of the 316L stainless steel"

Ferreira, M. O. A.; Mariani, F. E.; Leite, N. B.; Gelamo, R. V.; Aoki, I. V.; **Siervo, A. de*;** Pinto, H. C.; Moreto, J. A.

This work aims to investigate the influence of niobium and carbon nanostructured coatings on the corrosion resistance of the 316L SS. The coated and uncoated specimens were morphologically and structurally characterized by using OM, SEM/EDX, DRX, FTIR, Raman spectroscopy and XPS techniques. The corrosion behaviour was assessed by OCP, PPc, EIS as well as immersion tests in 0.6 mol L-1 NaCl solution. In addition, the average contact angles were used to evaluate the surfaces free energy by the Van Oss interfacial tension component theory approach.

Results showed that the surface treatments positively influenced the corrosion resistance of the 316L SS and the coatings act as a protective barrier against corrosion process. The reactive sputtering technique increased the wettability of the surfaces in relation to the base material. Considering applications in aggressive media, the 316L SS/Nb2O5 specimen exhibits superior performance when compared to the base material and 316L SS/carbon.

MATERIALS CHEMISTRY AND PHYSICS 312, 128610, 2024. DOI: 10.1016/j.matchemphys.2023.128610

[P012-2024] "Simulating selected magnetic properties of TbxPr1-x Al2, a magnetocaloric compound"

Tedesco, J. C. G.*; Jandre, V.; Carvalho, A. M. G.; Kockelmann, W.; Többens, D. M.; **Cardoso, L. P.***; **Coelho, A. A.***; Bordallo, H. N.

Tb- x Pr(1-x)Al(2)are ferrimagnetic materials exhibiting magnetocaloric effect that have gained considerable attention due to their potential use as an alternative in refrigeration, magnetic sensors and in information storage technology. Here using the mean field approach numerical simulations were conducted for x = 0.1, 0.2, 0.3, 0.4, 0.5, and 0.75, to analyze selected physical properties, such as x--ray and neutron powder diffraction, magnetization and heat capacity. The simulations successfully reproduced the experimental data providing a comprehensive characterization and improved understanding of this family of compound.

JOURNAL OF PHYSICS-CONDENSED MATTER 36[14], 145802, 2024. DOI: 10.1088/1361-648X/ad19a2

[P013-2024] "The quantum maxima for the basic graphs of exclusivity are not reachable in Bell scenarios"

Porto, L. E. A.*; Rabelo, R.*; Cunha, M. T.; Cabello, A.

A necessary condition for the probabilities of a set of events to exhibit Bell non-locality or Kochen-Specker contextuality is that the graph of exclusivity of the events contains induced odd cycles with five or more vertices, called odd holes, or their complements, called odd antiholes. From this perspective, events whose graph of exclusivity are odd holes or antiholes are the building blocks of contextuality. For any odd hole or antihole, any assignment of probabilities allowed by quantum theory can be achieved in specific contextuality scenarios. However, here we prove that, for any odd hole, the probabilities that attain the quantum maxima cannot be achieved in Bell scenarios. We also prove it for the simplest odd antiholes. This leads us to the conjecture that the quantum maxima for any of the building blocks cannot be achieved in Bell scenarios. This result sheds light on why the problem of whether a probability assignment is quantum is decidable, while whether a probability assignment within a given Bell scenario is quantum is, in general, undecidable. This also helps to understand why identifying principles for quantum correlations is simpler when we start by identifying principles for quantum sets of probabilities defined with no reference to specific scenarios.This article is part of the theme issue 'Quantum contextuality, causality and freedom of choice'.

PHILOSOPHICAL TRANSACTIONS OF THE ROYAL SOCIETY A-MATHEMATICAL PHYSICAL AND ENGINEERING SCIENCES 382[2268], 20230006, 2024. DOI: 10.1098/rsta.2023.0006

[P014-2024] "Thermal effusion of water and carbon oxides from multilayered graphene oxide thin films"

Silva, D. S. da*; Viana, G. A.*; Merlo, R. B.*; Silva, J. M. C. da*; Barros, T. A. S.; **Marques, F. C.***

We report on water (H2O) and carbon oxides (CO and CO2) effusion from multilayered graphene oxide (GO) films during thermal reduction. The effusion of molecules was monitored through the thermal desorption spectroscopy (TDS) technique in films prepared by evaporating a colloidal solution of GO. This method reduces the presence of adsorbed/trapped H2O molecules between adjacent GO planes. That allows the observation of additional effusion mechanisms. Thermal reduction process, from room temperature to similar to 1000 degrees C, was performed in a high-vacuum system with a mass spectrometer to monitor the outgassed species. A collective outgassing of H2O, CO2, CO species is observed and centered at approximately 230 degrees C. Above 400 degrees C, CO2 and CO are the only observed outgassed species. Multiple origins for water outgassing were inferred from the TDS spectrum asymmetry, revealing an intricate superposition of mechanisms. The thermal treatment also reduces both the GO interlayer separation and the film surface roughness.

MRS ADVANCES, 2024. DOI: 10.1557/s43580-024-00773-9. **Early Access Date: JAN 2024**

[P015-2024] "Who controls the curriculum? Notes on disciplinary communities from Ivor Goodson"

Petrucci-Rosa, M. I.; **Oiiveira, P. F. G.***

The present study investigates the devaluation of specialised teaching knowledge and the prioritisation of general education based on competencies and skills at the secondary level in Brazil. The dissolution of the curricular disciplinary organisation poses a risk to teaching identities, and understanding how teachers constitute epistemic and disciplinary communities is crucial. Public imposed policies that are distant from the reality of schools tend to be rejected by the agents involved in the school process. In Brazil, the National Curriculum Basis, a high school common core, is an example of a legal document that does not engage in dialogue with the cultural diversity in Brazil, while discredit the specific formation of teachers. From a historical approach, this research analyses the polysemy of school subjects towards the teacher's specialised identities. The methodological dispositive comprises narratives from specialist high school teachers in Biology, Physics, and Chemistry. Understanding how professionals organise themselves provides insight into the mechanisms of control and mediation in producing curriculum as socio-historical artifacts from power relationships and disputes. The struggle for control highlights the importance of teachers' agency in confrontation with neoliberal ideals for education and organising in subject or epistemic communities.

POLICY FUTURES IN EDUCATION, 2024. DOI: 10.1177/14782103241226529. **Early Access Date: JAN 2024**

[P016-2024] "X-ray photoelectron diffraction as a modern tool for determining surface stacking sequence in layered materials"

Lima, L. H. de; **Siervo, A. de***

We investigated the surface structure of a NbSe2 single crystal at room temperature, using angle-scanned x-ray photoelectron diffraction (XPD) combined with multiple scattering calculations. Different stacking sequences were tested (1T, 2H a , 2H c , and 3R), including possible stacking faults and a mixed 2H-3R stacking proposed earlier in the literature. We confirm the capability of XPD to distinguish different proposed structural models and, unambiguously, determine the true surface structure. Also, our findings provide reliable in-plane and interlayer distances.We observed expansions of the perpendicular distances between atomic planes within the monolayer and between monolayers of 3%-5%.

These results are important as accurate experimental input for the development of theoretical methods that involve a quantitative description of van der Waals systems.

2D MATERIALS 11[2], 025018, 2024. DOI: 10.1088/2053-1583/ad2526

***Autores da comunidade IFGW**
Fonte: Web of Science on-line (WOS)

Defesas de Dissertações do IFGW

[D001-2024] "Investigação das propriedades eletrônicas e estruturais de materiais topológicos sob aplicação de pressão uniaxial"
Aluno: Raphael Bonfim de Amorim François
Orientador: Profa. Dra. Cris Adriano
Data: 22/01/2024

[D002-2024] "Investigação da estabilidade de características baseadas em conectividade funcional dos sinais de EEG oriundos de imagética motora para aplicação em BCIs"
Aluno: Pedro Felipe Giarusso de Vazquez
Orientador: Profa. Dra. Gabriela Castellano
Data: 05/02/2024

[D003-2024] "Propriedades de Transporte Termoelétrico em Materiais half-Heusler através de Métodos Ab Initio"
Aluno: Mateus Corradini Lopes
Orientador: Prof. Dr. Alex Antonelli
Data: 08/03/2024

[D004-2024] "Um Estudo sobre as Correlações Quase Quânticas"
Aluno: Vitor Lucas de Oliveira Sena
Orientador: Prof. Dr. Rafael Luiz da Silva Rabelo
Data: 19/03/2024

[D005-2024] "Análise Combinada dos Sinais de Carga e Luz na Detecção de Neutrinos Oscilados no Experimento DUNE"
Aluno: Luís Gustavo Porto Paixão
Orientador: Prof. Dr. Ettore Segreto
Data: 25/03/2024

[D006-2024] "Estudo da produção da heteroestrutura de MoS2 -WSe2 e acoplamento da sua fotoluminescência em guias de onda de Silício"
Aluno: Kalebe Batista Estevam
Orientador: Prof. Dr. Pierre Louis de Assis
Data: 27/03/2024

Defesas de Teses do IFGW

[T001-2024] "Sondando o papel dos elétrons 4f no estado fundamental dos supercondutores férmions pesados CeCu2 Si2 e RPt4 Ge12 (R = La, Pr) usando radiação síncrotron"
Aluno: Gustavo Aparecido Lombardi
Orientador: Prof. Dr. Ricardo Donizeth dos Reis
Data: 16/01/2024

[T002-2024] "Aplicações do modelo de Derrida-Higgs finito em dinâmica de populações"
Aluno: Vítor Marquioni Monteiro
Orientador: Prof. Dr. Marcus Aloizio Martinez de Aguiar
Data: 23/02/2024

[T003-2024] "Nano-Óptica de Poláritons e Radiação Térmica de Materiais Bidimensionais em Campo-Próximo no Regime de Infravermelho"
Aluno: Flavio Henrique Feres
Orientador: Prof. Dr. Francisco Carlos Barbosa Maia
Data: 14/03/2024

Fonte: Portal IFGW/Eventos
Disponível em: https://portal.ifi.unicamp.br/a-instituicao/eventos/month.calendar/2023/12/14/-

Defesas de Dissertações e Teses do PECIM

[P001-2024] "Ensino de ciências e matemática sob a ótica da teoria cognitiva de aprendizagem multimídia: tendências de pesquisa acadêmica no Brasil e na América Latina"
Aluno: Iago Braga da Silva
Orientador: Prof. Dr. Samuel Rocha de Oliveira
Banca: Prof Dr Samuel Rocha de Oliveira - IMECC/Unicamp (Presidente), Dr Valdinei Cezar Cardoso - UFES, **Prof Dr Guilherme Stecca Marcom - IFGW/Unicamp,** Dra Ana Paula Jahn - IME/USP (Suplente), Profa Dra Alessandra Aparecida Viveiro - FE/Unicamp (Suplente)
Data: 27/02/2024
Exame de Defesa: Mestrado

Fonte: Página do PECIM
Disponível em: https://www.pecim.unicamp.br/bancas

Abstracta

Instituto de Física
Diretor: Profa. Dra. Mônica Alonso Cotta
Diretora Associada: Prof. Dr. Marcos Cesar de Oliveira
Universidade Estadual de Campinas - UNICAMP
Cidade Universitária Zeferino Vaz
13083-859 - Campinas - SP - Brasil
e-mail: secdir@ifi.unicamp.br
Fone: +55 19 3521-5300

Publicação

Biblioteca do Instituto de Física Gleb Wataghin
http://portal.ifi.unicamp.br/biblioteca
Instagram: @bif.unicamp

Diretora Técnica: Sandra Maria Carlos Cartaxo
Coordenadora da Comissão de Biblioteca: Profa. Dra. Arlene Cristina Aguilar

Elaboração e editoração:
Maria Graciele Trevisan (Bibliotecária)
Artes gráficas:
Júlia da Silva Oliveira (Estagiária)
contato: infobif@ifi.unicamp.br